Cytoplasmic sharing through apical membrane remodeling

Nora G. Peterson[1], Benjamin M. Stormo[1], Kevin P. Schoenfelder[2], Juliet S. King[3], Rayson R. S. Lee[4], Donald T. Fox[1,2,3,*]

1. Department of Cell Biology, Duke University Medical Center, Durham NC USA 27710
2. University Program in Genetics and Genomics, Duke University, Durham NC 27710
3. Department of Pharmacology & Cancer Biology, Duke University Medical Center, Durham NC USA 27710
4. Duke-NUS Medical School, 169857 Singapore, Singapore.

*Correspondence to: don.fox@duke.edu

ONE SENTENCE SUMMARY

Apical membrane remodeling in a resorptive *Drosophila* epithelium generates a shared multinuclear cytoplasm.

ABSTRACT

Multiple nuclei sharing a common cytoplasm are found in diverse tissues, organisms, and diseases. Yet, multinucleation remains a poorly understood biological property. Cytoplasm sharing invariably involves plasma membrane breaches. In contrast, we discovered cytoplasm sharing without membrane breaching in highly resorptive *Drosophila* rectal papillae. During a six-hour developmental window, 100 individual papillar cells assemble a multinucleate cytoplasm, allowing passage of proteins of at least 27kDa throughout papillar tissue. Papillar cytoplasm sharing does not employ canonical mechanisms such as failed cytokinesis or muscle fusion pore regulators. Instead, sharing requires gap junction proteins (normally associated with transport of molecules <1kDa), which are positioned by membrane remodeling GTPases. Our work reveals a new role for apical membrane remodeling in converting a multicellular epithelium into a giant multinucleate cytoplasm.

MAIN TEXT

Sharing of cytoplasm in a multinucleate tissue or organism is an important and recurring adaptation across evolution. Multinucleate structures include animal skeletal muscle, mammalian osteoclasts, and mammalian syncytial placental trophoblasts (*1-3*). In disease, cytoplasm sharing facilitates the spread of pathogens (*4*), oncogenic factors (*5, 6*), and prion-like proteins (*7*). Cytoplasm sharing can occur through cytokinesis failure, or through plasma membrane breaches such as fusion pores, tunneling nanotubes, or plasmodesmata. Such clearly visible breaches enable exchange of cytoplasmic components such as RNA, proteins, and even organelles (*8, 9*). The ubiquity and importance of cytoplasm sharing led us to seek out novel examples in the tractable animal model *Drosophila melanogaster.* Here, we report an animal-wide screen for tissues that share cytoplasm. We identify a novel mechanism of cytoplasm sharing in the rectal papilla, a resorptive intestinal epithelium (*10*) and known site of pathogen localization (*11*). Unlike all known examples of multinucleation, cytoplasm sharing in rectal papillae involves developmentally programmed apical membrane remodeling.

To identify new examples of adult tissues in *Drosophila* that share cytoplasm, we ubiquitously expressed *UAS-dBrainbow* (*12*) (**Fig1A**), a Cre-Lox-based system that randomly labels cells with only one of three fluorescent proteins. Multi-labeled cells should only arise by fusion of cells not related by cell division/cytokinesis failure (**Fig1B**). We examined a wide range of tissues (**FigS1A**). From our screen, we discovered that the rectal papilla is a new example of a tissue with cytoplasm sharing. Adult *Drosophila* contain four papillae, each with 100 nuclei, that reside in the posterior hindgut (**Fig1C**). Using both fixed and live imaging of whole organs, we found that at 62 hours post puparium formation (HPPF), each papillar cell contains only one dBrainbow label (**Fig1D**). By contrast, at 69HPPF, multi-labeled cells are apparent (**Fig1D',F-F'**). We quantitatively measured papillar sharing across the tissue (**FigS1B**, *Methods*) and found that cytoplasm sharing initiates over a narrow 6-hour period (68-74HPPF, **Fig1E**). Our results suggested that at least

RNA and possibly protein passes between papillar cells to facilitate cytoplasm sharing. To directly test if protein is shared, we photo-activated GFP (PA-GFP) in single adult papillar cells and observed in real time whether GFP spreads to adjacent cells. We find the principal papillar cells, but not the secondary cells at the papillar base ((*13*), **FigS1C**), share protein across an area of at least several nuclei (**Fig1G-H**). Therefore, proteins as large as ~27kDa (the size of GFP) can move across an area covered by multiple papillar nuclei. These results indicate that papillae undergo a developmentally programmed conversion from 100 individual cells to a single multinuclear cytoplasm.

We next examined whether cytoplasm sharing requires the distinctive papillar cell cycle program, which completes prior to sharing onset (**FigS1D**). Larval papillar cells first undergo endocycles, which increase cellular ploidy, and then pupal papillar cells undergo polyploid mitotic cycles, which increase cell number (*14*). Knockdown of the endocycle regulator *fizzy-related* (*15*) significantly disrupts cytoplasm sharing (**FigS1E,F,H**). We hypothesize that endocycles are required for differentiation of the papillae, which later enables these cells to trigger cytoplasm sharing. In contrast, blocking Notch signaling, which initiates papillar mitotic divisions (*14*), does not prevent sharing (**FigS1E,G,H**). Thus, papillar cytoplasm sharing requires developmentally programmed endocycles but not mitotic cycles.

As our *dBrainbow* approach only identifies cytoplasm sharing events that do not involve failed division/cytokinesis, we examined whether sharing results from fusion pore formation, as in skeletal muscle. A well-studied model of such cell-cell fusion in *Drosophila* is myoblast fusion, which requires an actin-based podosome (*16, 17*). We conducted a candidate *dBrainbow*-based RNAi screen (77 genes, **Fig2A, Table S1**) of myoblast fusion regulators and other plasma membrane components. Remarkably, 0/15 myoblast fusion genes from our initial screen regulate papillar cytoplasm sharing (**Fig2A**, **FigS2A**, **Table S1**). Furthermore, dominant-negative forms of

Rho family GTPases have no impact on Brainbow labeling (**FigS2B**), providing additional evidence against actin-based cytoplasm sharing. Instead, we found 8/77 genes, including subunits of the vacuolar H+ ATPase (*Vha16-1*), ESCRT-III complex (*Vps2*), and exocyst (*Exo84*) (**Fig2A**) are required for papillar cytoplasm sharing. Through additional screening, the only myoblast fusion regulator required for papillar cytoplasm sharing is *singles bar* (*sing*), a presumed vesicle trafficking gene (*18*) (**FigS2A**). Given the enrichment of our candidate screen hits in membrane trafficking and not myoblast fusion, we further explored the role of membrane trafficking in cytoplasm sharing.

We conducted two secondary dBrainbow screens to find specific membrane trafficking pathway components that regulate papillar sharing. First, a focused candidate membrane trafficking screen revealed additional components (12/36 genes screened, **Fig2B, Table S2**) including 3 more vacuolar H+ ATPase subunits, 5 more exocyst components, and the Dynamin GTPase *shibire* (*shi*) (**Fig2B,D,E,H**). Second, we screened constitutively-active and dominant-negative versions of all 31 *Drosophila* Rabs. Sharing requires only a small number of Rabs, specifically the ER/Golgi-associated *Rab1,* the early endosome-associated *Rab5,* and the recycling endosome-associated *Rab11* (**Fig2C,D,F-H**). Given our identification of the membrane vesicle recycling circuit involving *shi*, *Rab5*, and *Rab11*, we focused on these genes. Two unique RNAi lines for each gene show consistent sharing defects, and most of these knockdowns completely recapitulate the pre-sharing state (**Fig2H**). Despite exhibiting strong cytoplasm sharing defects, *shi*, *Rab5*, and *Rab11 RNAi* papillae appear morphologically normal, with only minor cell number decreases (**FigS2C**). These results suggest that membrane recycling GTPases regulate a specific developmental event associated with cytoplasm sharing, and not papillar morphogenesis. In agreement with these GTPases acting during development, rather than as part of an ongoing transport process, GTPase knockdown after sharing onset does not block cytoplasm sharing (**FigS2D-F**). Together, our screens reveal that membrane trafficking, particularly Dynamin-

mediated endocytosis and early/recycling endosome trafficking, regulates papillar cytoplasmic sharing.

To better understand how membrane trafficking GTPases initiate cytoplasm sharing during development, we examined endosome and Shi localization during sharing onset. We imaged a GFP-tagged pan-endosome marker (*myc-2x-FYVE*) and a Venus-tagged *shi* before and after sharing. Endosomes are evenly distributed shortly before sharing, but become highly polarized at the basal membrane around the time of sharing onset (**Fig3A-A',C, FigS3A**). This basal endosome repositioning requires Shi (**Fig3B-C, FigS3A**) and the change in endosome localization is attributed to Rab5-positive early endosomes (**FigS3B-C**). Additionally, Shi localization changes from apical polarization to a uniform distribution during sharing onset (**Fig3D-E**). These localization changes indicate that membrane trafficking factors are dynamic during cytoplasm sharing onset.

To determine what membrane remodeling events underlie GTPase-dependent cytoplasm sharing, we turned to ultrastructural analysis. Adult ultrastructure and physiology of papillar cells has been examined previously in *Drosophila* (*19*) and related insects (*20*). These cells contain elaborate membrane networks that facilitate selective ion resorption from the gut lumen, facing the apical side of papillar cells, to the hemolymph, facing the basal side. Still, little is known about developmental processes or mechanisms governing the unique papillar cell architecture. We looked for changes in cell-cell junctions and lateral membranes that coincide with cytoplasm sharing, especially to determine if there is a physical membrane breach between cells. We identified several dramatic changes in membrane architecture. First, apical microvilli-like structures form during sharing onset (**Fig3F-F''**). Just basal to the microvilli, apical cell-cell junctions compress from a straight to a more tortuous morphology around the time of cytoplasm sharing onset **(FigS3D-D''**). One of the most striking changes, coincident with Shi re-localization,

is formation of pan-cellular endomembrane stacks surrounding mitochondria. These stacks are likely ion transport sites (**Fig3G-G''**). Thus, massive apical and intracellular plasma membrane reorganization coincides with both cytoplasm sharing and Shi/endosome re-localization. We next assessed whether the extensive membrane remodeling requires Shi, Rab5, and Rab11. In *shi* and *Rab5 RNAi* animals, microvilli protrude downward, instead of upward (**Fig3H-J**). Additionally, apical junctions do not compress as in controls (**FigS3E-G**). Notably, membrane stacks are greatly reduced (**Fig3K-M**). *shi RNAi* animals exhibit numerous trapped vesicles, consistent with a known role for Dynamin in membrane vesicle severing (*21, 22*) (**Fig3L, inset**). Together, we find that Shi and endosomes extensively remodel membranes during cytoplasm sharing.

Our extensive ultrastructural analysis did not reveal any clear breaches in the plasma membrane, despite numerous membrane alterations. Adult papillae exhibit large extracellular spaces between nuclei that eliminate the possibility of cytoplasm sharing throughout much of the lateral membrane (**FigS4A**) (*19, 20*). Instead, through our GTPase knockdown studies, we identified a striking alteration in the apical cell-cell interface that strongly correlates with cytoplasm sharing. Specifically, *shi* animals frequently lack apical gap junctions (**Fig3N-O**) ($p<0.0001$) (**Fig3P**, **FigS3H-H''**). Upon closer examination of control animal development, we find that apical gap junction-like structures arise at cytoplasm sharing onset. There is almost no gap junction-like structure before cytoplasm sharing (**Fig4A-B**, **FigS5A-A''**). Given our electron micrograph results, we determined which innexins, the protein family associated with gap junctions in invertebrates (*23, 24*), are expressed in rectal papillae. From RNA-seq data (*Methods*), we determined that *ogre* (*Inx1*), *Inx2*, and *Inx3* are most highly expressed (**Fig4C**). This combination of innexins is not unique; the non-sharing brain and optic lobe (**FigS1A**) also express high levels of all three (*25*). We examined localization of Inx3 (a gap junction component), and compared it to a septate junction component, NeurexinIV (NrxIV). NrxIV localizes similarly both pre and post-sharing onset (**Fig4D-D'**), indicative of persistent septate junctions remaining between papillar cells. In contrast,

Inx3 organizes apically only after cytoplasm sharing (**Fig4E-E'**, **FigS5B-B'**). We tested whether innexins are required for cytoplasm sharing. Knocking down these three genes individually causes mild yet significant cytoplasm sharing defects (**Fig4F**). However, we see larger defects when we express dominant-negative $ogre^{DN}$ (**Fig4F-G**), which contains a C-terminal GFP tag that interferes with channel passage. Also, heterozygous animals containing a ten gene-deficiency spanning *ogre*, *Inx2*, and *Inx7* have more severe defects (**Fig4F**, *Df(1)BSC867*). Finally, we tested whether cytoplasm sharing is essential for normal rectal papillar function. Rectal papillae selectively absorb water and ions from the gut lumen for transport back into the hemolymph, and excrete unwanted lumen contents. One test of papillar function is viability following the challenge of a high-salt diet (*15, 26*). Using either pan-hindgut or papillae-specific (**FigS5C-D,** *Methods*) knockdown of cytoplasm sharing regulators, we find both shi^{DN} and $ogre^{DN}$ animals are extremely sensitive to the high-salt diet (mean survival <1 day, **Fig4H**). These results underscore an important function for gap junction proteins, as well as membrane remodeling by Shibire, in cytoplasm sharing.

Our findings identify *Drosophila* rectal papillae as a new and distinctive example of cytoplasm sharing in a simple, genetically tractable system. Papillar cytoplasm sharing is developmentally regulated, occurring over a brief 6-hour window, and requires membrane remodeling by trafficking GTPases, which apically position gap junction proteins (**Fig4I, FigS5H**). These membrane and junctional changes are required for normal rectum function. We speculate that papillar cytoplasm movement across a giant multinuclear structure enhances resorption by facilitating interaction of ions and ion transport machinery with intracellular membrane stacks. Given the absence of other clear canals, channels, or breaks in lateral membrane, our data suggest a specialized function of gap junction proteins facilitates cytoplasm sharing between neighboring cells in an otherwise intact epithelium (**Fig4I**). Although gap junctions typically transfer molecules of <1kDa, elongated proteins up to 18 kDa are observed to pass through certain vertebrate gap junctions (*27*). Our

results have several implications for functions and regulation of multinucleation. Given that cytoplasm sharing facilitates pathogen spread (*4*), and that papillae are an avenue of entry for mosquito viruses (*11*), our findings may impact insect vector control strategies. Our prior work (*15*) revealed that papillae are highly tolerant of chromosome mis-segregation, and our work here suggests this tolerance may be due in part to neutralization of aneuploidies through cytoplasm sharing, a finding relevant to syncytial cancers. In the future, our Brainbow-based approach could be applied to other contexts to identify other tissues with gap junction-dependent but membrane breach-independent cytoplasm sharing. Collectively, our findings highlight the expanding diversity of multicellular tissue organization strategies.

REFERENCES AND NOTES

1. S. Deng, M. Azevedo, M. Baylies, Acting on identity: Myoblast fusion and the formation of the syncytial muscle fiber. *Semin Cell Dev Biol* **72**, 45-55 (2017).
2. P. Gerbaud, G. Pidoux, Review: An overview of molecular events occurring in human trophoblast fusion. *Placenta* **36 Suppl 1**, S35-42 (2015).
3. M. Pereira *et al.*, Common signalling pathways in macrophage and osteoclast multinucleation. *J Cell Sci* **131**, (2018).
4. E. A. Eugenin, P. J. Gaskill, J. W. Berman, Tunneling nanotubes (TNT) are induced by HIV-infection of macrophages: a potential mechanism for intercellular HIV trafficking. *Cell Immunol* **254**, 142-148 (2009).
5. E. Lou *et al.*, Tunneling nanotubes provide a unique conduit for intercellular transfer of cellular contents in human malignant pleural mesothelioma. *PLoS One* **7**, e33093 (2012).
6. J. Lu *et al.*, Tunneling nanotubes promote intercellular mitochondria transfer followed by increased invasiveness in bladder cancer cells. *Oncotarget* **8**, 15539-15552 (2017).
7. K. Gousset *et al.*, Prions hijack tunnelling nanotubes for intercellular spread. *Nat Cell Biol* **11**, 328-336 (2009).
8. A. Rustom, R. Saffrich, I. Markovic, P. Walther, H. H. Gerdes, Nanotubular highways for intercellular organelle transport. *Science* **303**, 1007-1010 (2004).
9. P. F. McLean, L. Cooley, Protein equilibration through somatic ring canals in Drosophila. *Science* **340**, 1445-1447 (2013).
10. V. B. Wigglesworth, On the function of the so-called 'rectal glands' of insects. *Q J Microsc Sci* **75**, 131-150 (1932).
11. J. B. Gu, Y. Q. Dong, H. J. Peng, X. G. Chen, A recombinant AeDNA containing the insect-specific toxin, BmK IT1, displayed an increasing pathogenicity on Aedes albopictus. *Am J Trop Med Hyg* **83**, 614-623 (2010).
12. S. Hampel *et al.*, Drosophila Brainbow: a recombinase-based fluorescence labeling technique to subdivide neural expression patterns. *Nat Methods* **8**, 253-U102 (2011).
13. M. Garayoa, A. C. Villaro, M. J. Lezaun, P. Sesma, Light and electron microscopic study of the hindgut of the ant (Formica nigricans, Hymenoptera): II. Structure of the rectum. *J Morphol* **242**, 205-228 (1999).
14. D. T. Fox, J. G. Gall, A. C. Spradling, Error-prone polyploid mitosis during normal Drosophila development. *Gene Dev* **24**, 2294-2302 (2010).
15. K. P. Schoenfelder *et al.*, Indispensable pre-mitotic endocycles promote aneuploidy in the Drosophila rectum. *Development* **141**, 3551-3560 (2014).
16. B. E. Richardson, K. Beckett, S. J. Nowak, M. K. Baylies, SCAR/WAVE and Arp2/3 are crucial for cytoskeletal remodeling at the site of myoblast fusion. *Development* **134**, 4357-4367 (2007).
17. K. L. Sens *et al.*, An invasive podosome-like structure promotes fusion pore formation during myoblast fusion. *J Cell Biol* **191**, 1013-1027 (2010).
18. B. Estrada *et al.*, The MARVEL domain protein, Singles Bar, is required for progression past the pre-fusion complex stage of myoblast fusion. *Dev Biol* **307**, 328-339 (2007).
19. A. Wessing, D. Eichelberg, [Electron microscopic studies on structure and function of the rectal papillae in Drosophila melanogaster]. *Z Zellforsch Mikrosk Anat* **136**, 415-432 (1973).
20. B. L. Gupta, M. J. Berridge, Fine Structural Organization of Rectum in Blowfly Calliphora Erythrocephala (Meig) with Special Reference to Connective Tissue Tracheae and Neurosecretory Innervation in Rectal Papillae. *J Morphol* **120**, 23-+ (1966).
21. H. Damke, T. Baba, D. E. Warnock, S. L. Schmid, Induction of Mutant Dynamin Specifically Blocks Endocytic Coated Vesicle Formation. *J Cell Biol* **127**, 915-934 (1994).

22. J. E. Hinshaw, S. L. Schmid, Dynamin Self-Assembles into Rings Suggesting a Mechanism for Coated Vesicle Budding. *Nature* **374**, 190-192 (1995).
23. R. Bauer *et al.*, Intercellular communication: the Drosophila innexin multiprotein family of gap junction proteins. *Chem Biol* **12**, 515-526 (2005).
24. P. Phelan *et al.*, Drosophila Shaking-B protein forms gap junctions in paired Xenopus oocytes. *Nature* **391**, 181-184 (1998).
25. D. P. Leader, S. A. Krause, A. Pandit, S. A. Davies, J. A. T. Dow, FlyAtlas 2: a new version of the Drosophila melanogaster expression atlas with RNA-Seq, miRNA-Seq and sex-specific data. *Nucleic Acids Res* **46**, D809-D815 (2018).
26. H. S. Bretscher, D. T. Fox, Proliferation of Double-Strand Break-Resistant Polyploid Cells Requires Drosophila FANCD2. *Dev Cell* **37**, 444-457 (2016).
27. A. M. Cieniewicz, R. I. Woodruff, Passage through vertebrate gap junctions of 17/18 kDa molecules is primarily dependent upon molecular configuration. *Tissue Cell* **42**, 47-52 (2010).

ACKNOWLEDGMENTS

We thank members of the Fox laboratory and Drs. Dong Yan and Tony Harris for valuable feedback. Ying Hao (Duke Eye Center) provided assistance with electron microscopy. **Funding:** This work was supported by NIH grants GM118447 to D.F. and HL140811 to N.P. **Author contributions:** experimental design, execution, and data analysis- all authors, manuscript writing and editing- N.P. and D.F. **Competing interests-** authors declare no competing interests. **Data and materials availability-** all data is available in the main text or the supplementary materials.

MAIN FIGURE LEGENDS

Figure 1. Developmentally programmed cytoplasmic sharing in *Drosophila* papillae.

(**A**) dBrainbow. Cre recombinase randomly excises one pair of lox sites, and approximately 1/3 of cells express either EGFP, mKO2, or mTFP1. (**B**) Model of dBrainbow expression with no, partial, or complete cytoplasmic sharing. (**C**) *Drosophila* digestive tract with rectum containing four papillae labeled in magenta box. (**D-D''**) Representative *dBrainbow* papillae at 62 (**D**), 69 (**D'**), or 80 (**D''**) hours post-puparium formation (HPPF). (**E**) Cytoplasmic sharing quantification during pupal development. Lines= mean at each time, which differs significantly between 66 and 74 HPPF ($p<0.0001$). Each point=1 animal (N=9-18, rep=2). (**F**) Live *dBrainbow*-labelled papillar cells during cytoplasmic sharing (69 HPPF). (**F'**) Fluorescence of neighboring cells in (**F**). (**G-H**) Representative adult papilla expressing photo-activatable GFP (PA-GFP). Single cells were photo-activated (yellow X) in secondary cells (**G**) and principal cells (**H**). Time=seconds after activation.

Figure 2. Cytoplasmic sharing requires membrane remodeling proteins.

(**A**) Primary *dBrainbow* candidate screen. RNAi and dominant-negative versions of 77 genes representing the indicated roles were screened for sharing defects, and 8 genes were identified. (**B**) Secondary membrane trafficking screen. 36 genes were screened with 12 sharing genes identified. (**C**) Secondary screen of dominant-negative and constitutively-active Rab GTPases. (**D-G**) Representative *dBrainbow* in (**D-D'**) wild type (WT) (**D**) pre-sharing (48HPPF) and (**D'**) post-sharing (young adults), (**E**) adult *shi RNAi,* (**F**) adult *Rab5 RNAi*, (**G**) adult *Rab11 RNAi*. (**H**) Quantification of **D-G**, including two RNAi lines for *shi*, *Rab5*, and *Rab11*. Pre-sharing and knock downs differ significantly from post-sharing WT ($p<0.0001$, N=9-32, rep=2-3).

Figure 3. Gap junction establishment, but no membrane breaches, accompany cytoplasm sharing.

(**A-A'**) Endosome localization (GFP-myc-2x-FYVE), representative of (**A**) pre- and (**A'**) post-sharing onset. (**B**) Endosomes in *shi RNAi* post-sharing, *see Methods*. (**C**) Aggregated endosome line profiles for WT pre-sharing (N=6, rep=3), WT post-sharing (N=7, rep=2), and *shi RNAi* post-sharing (N=10, rep=2). Shaded area represents standard error. (**D-D'**) Shi-Venus localization pre- and post-sharing onset. (**E**) Line profiles as in (**D-D'**) (N=4-5, rep=3). (**F-O**) Representative Transmission Electron Micrographs (TEMs). **(F-F'')** Microvillar-like structures (MV) pre (**F**), mid- (**F'**), and post- (**F''**) sharing onset. (**G-G''**) Mitochondria and surrounding membrane pre- (**G**), mid- (**G'**), and post- (**G''**) sharing onset. (**H-J**) Microvillar-like structures (MV) of adult papillae in WT (**H**), *shi RNAi* (**I**), and *Rab5 RNAi* (**J**). (**K-M**) Mitochondria and surrounding membranes of adult papillae in WT (**K**), *shi RNAi* (**L**), and *Rab5 RNAi* (**M**). Inset in **L** shows trapped vesicles. (**N-O**) WT and *shi RNAi* post-sharing. Adherens (orange), septate (green), and gap (blue) junctions are highlighted. (**P**) Quantification of the ratio of gap junction length to septate plus gap junction length (Fraction gap junction) (N=3-4, rep=2). $p<0.0001$ for the difference in gap junction ratio between WT and *shi RNAi*.

Figure 4. Gap junction proteins are required for cytoplasmic sharing.

(**A-A''**) Representative apical junctions highlighted by junctional type in pre (**A**), mid (**A'**), and post (**A''**) sharing onset. (**B**) Quantification of fraction gap junction (gap junction length / (gap + septate junction length)) in pre-, mid-, and post-sharing onset pupae (N=3-4, rep=2). (**C**) *Drosophila* innexin expression in the adult rectum (*Methods*). (**D-D'**) Adherens junctions in pre- (**D**) and post- (**D'**) sharing pupae visualized by *NrxIV-GFP*. (E-E') WT pupae pre- and post-sharing onset stained with anti-Inx3. (**F**) Quantification of cytoplasm sharing in WT, $ogre^{DN}$, *Df(1)BSC867/+* (a 10-gene deficiency covering *ogre*, *Inx2*, and *Inx7*), and *ogre RNAi* adult papillae (N=13-14, rep=2). (**G**) Representative adult rectal papilla expressing *GFP-ogre* and *dBrainbow*. (**H**) Survival of WT,

shi^{DN}, and *ogre*^{DN} animals on a high-salt diet (N=27-37, rep=3). (**I**) Proposed model for cytoplasmic sharing in an intact papillar epithelium.

List of supplementary materials

Materials and Methods

Table S1-S6

Fig S1-S5

References (27-42)

Figure 1

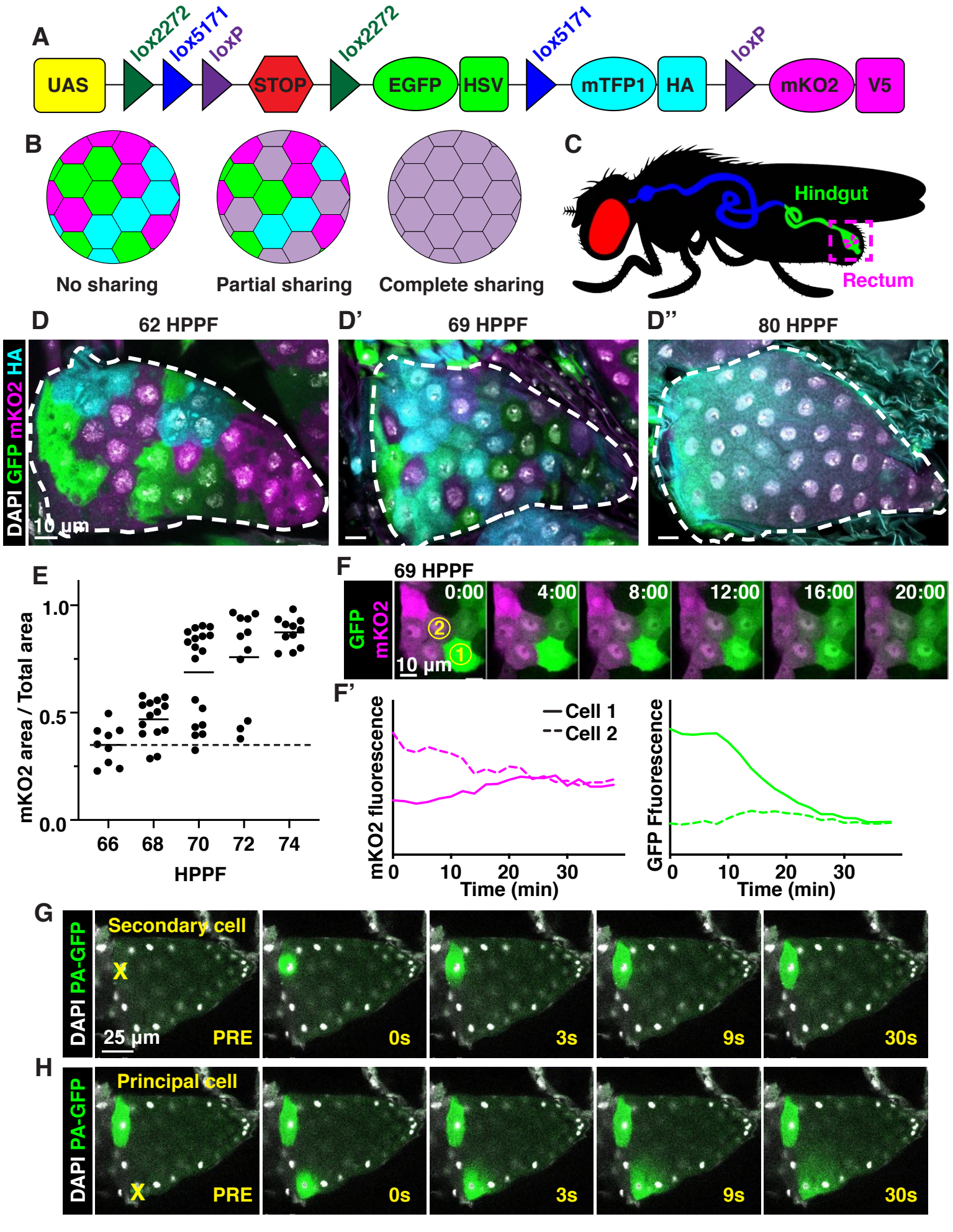

Figure 2

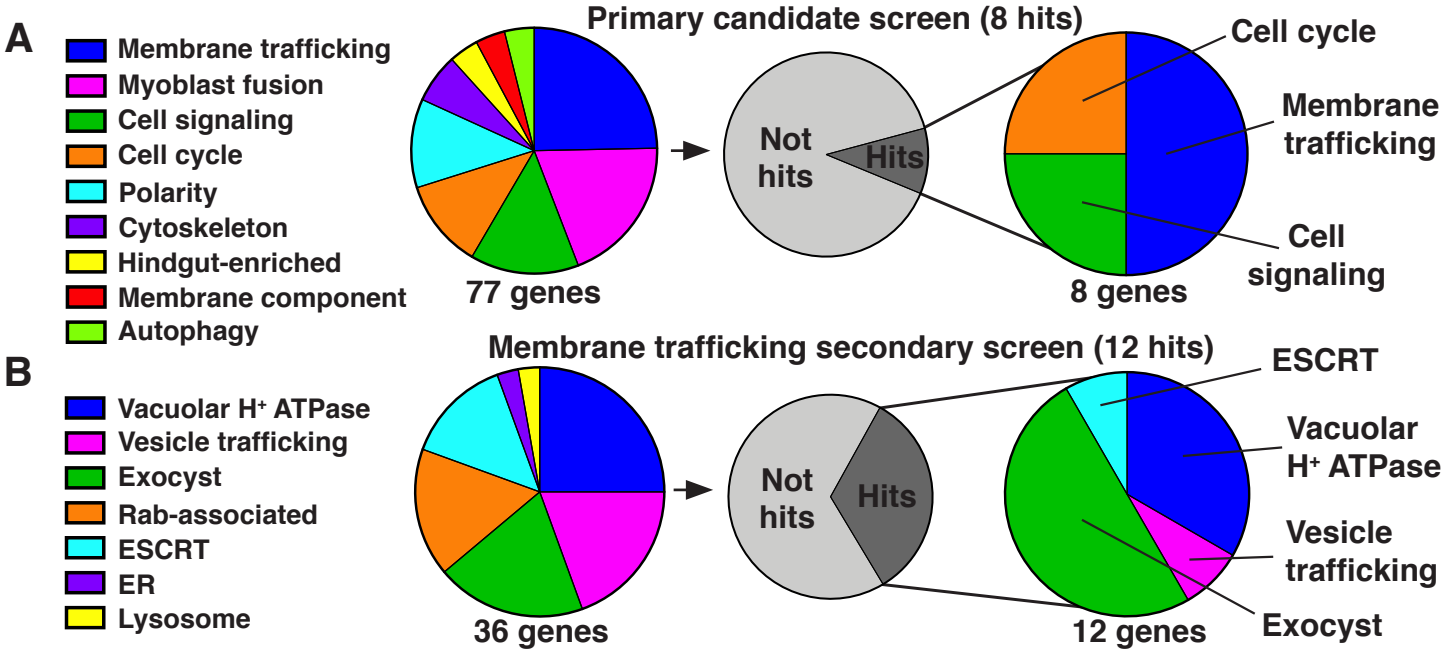

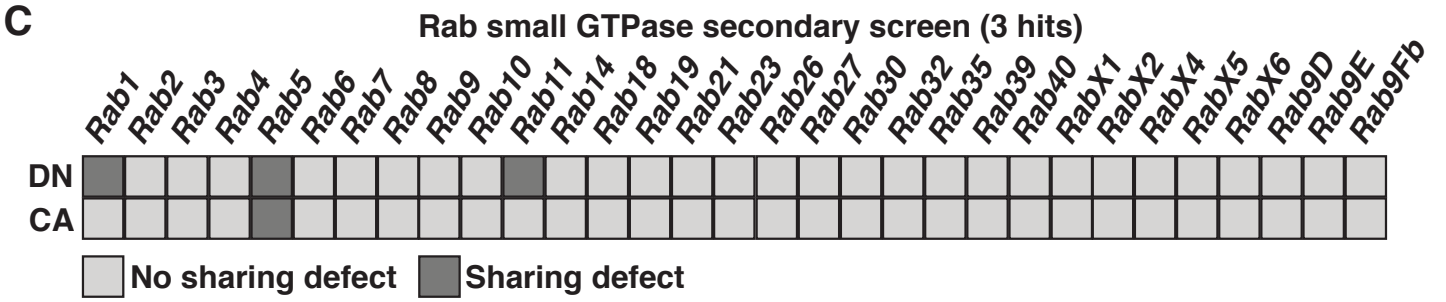

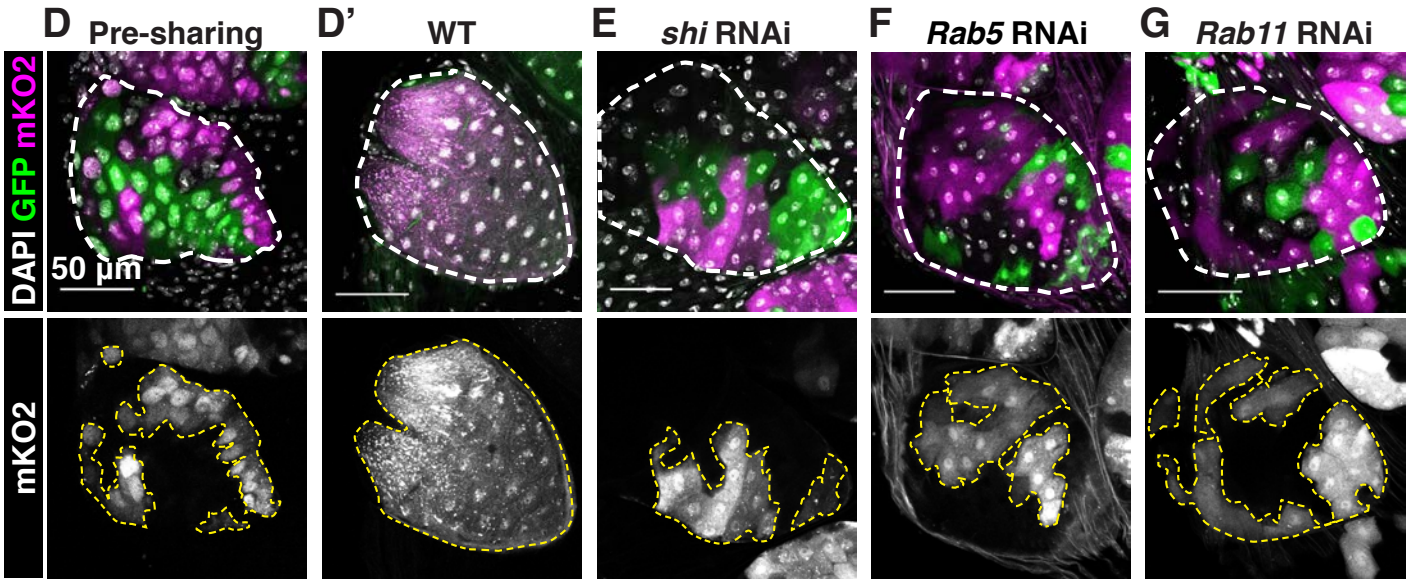

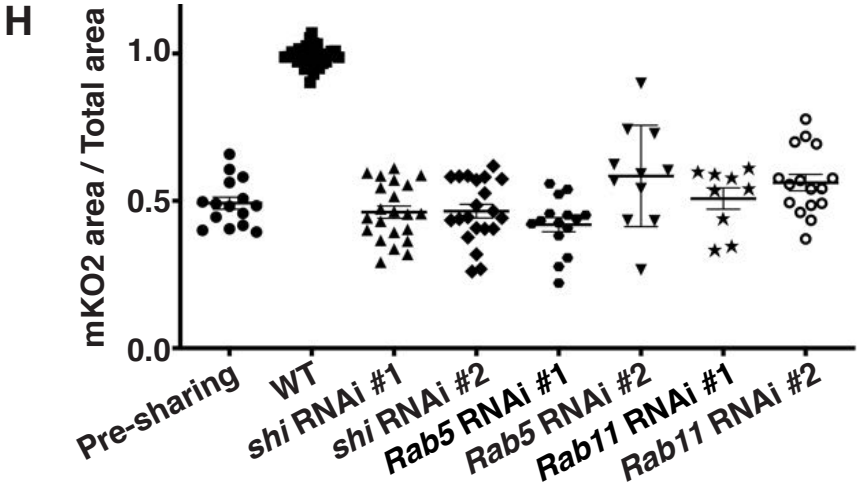

Figure 3

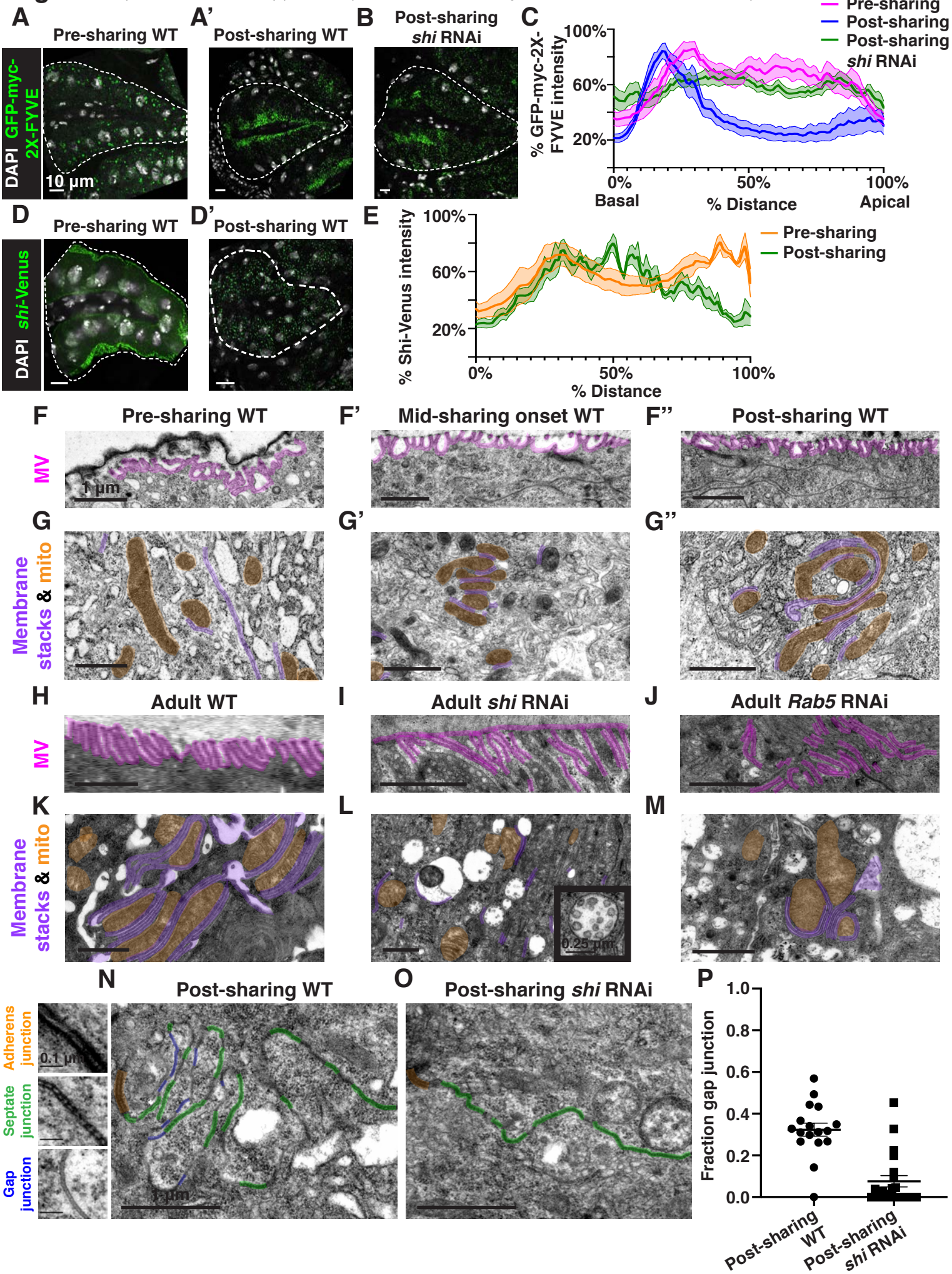

Figure 4

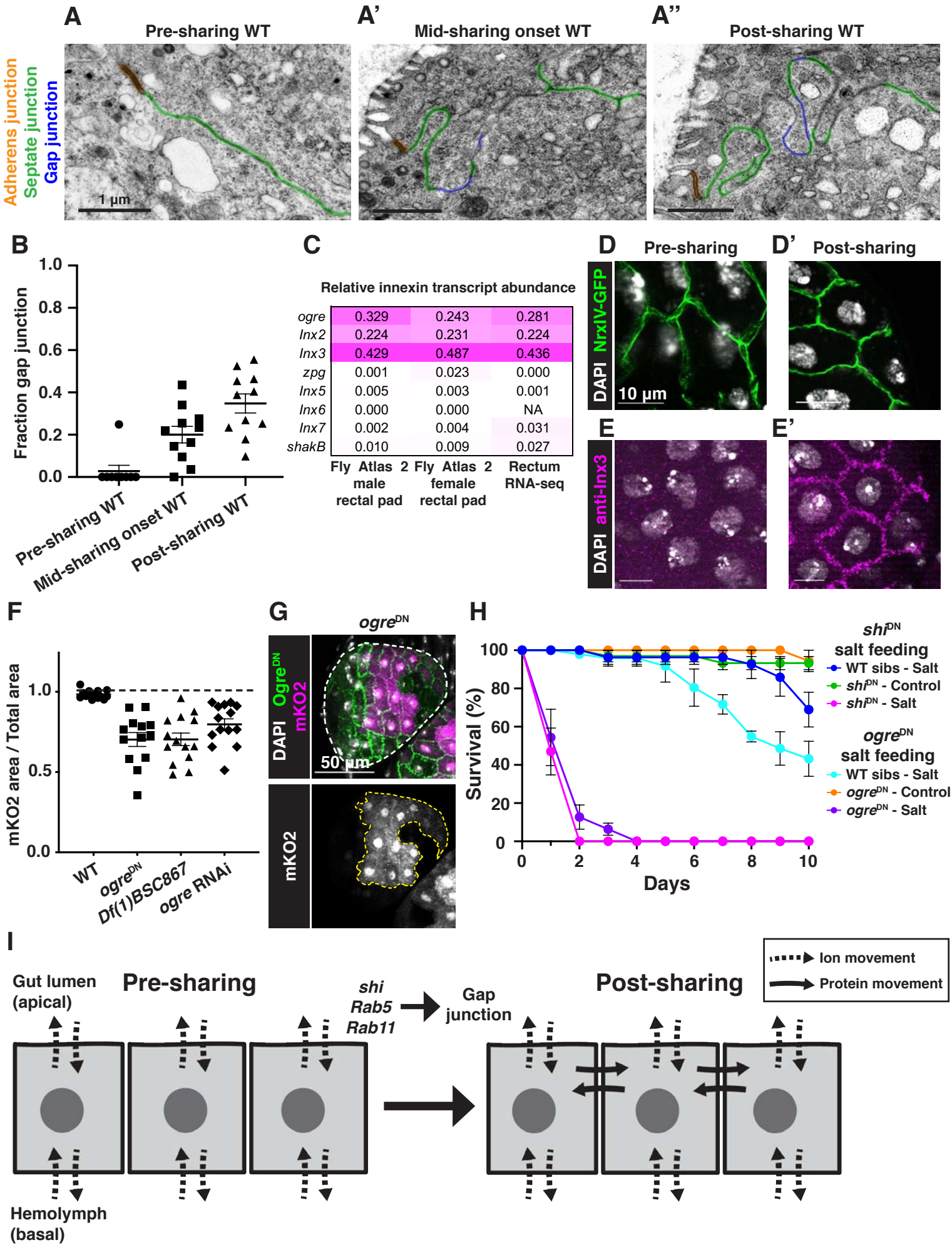

SUPPLEMENTARY MATERIAL

MATERIALS AND METHODS

Fly Stocks and Genetics

Flies were raised at 25C on standard media (Archon Scientific, Durham, NC) unless specified otherwise. See **Table S4** for a list of fly stocks used. See **Table S3** for a full list of fly lines screened in primary and secondary screens. See **Table S5** for panel-specific genotypes.

brachyenteron (byn)-Gal4 was the driver for all UAS transgenes with the exception of the screen in **FigS1A**, which used *Tubulin-Gal4*, and the *shi* knockdown in **Fig4H**, which used *60H12-Gal4*. *60H12-Gal4* expresses only in the papillar cells and not the rest of the hindgut, and use of this driver blocks cytoplasm sharing using *UAS-shi^{DN}* (**FigS5C-G**). For all *Gal4* experiments, *UAS* expression was at 29C, except in **Fig1D-F**, where it was at 25C. If *byn-Gal4* expression of a given *UAS*-transgene was lethal, the experiment was repeated with a temperature-sensitive *Gal80^{ts}* repressor transgene and animals were kept at 18C until shifting to 29C at an experimentally-determined time point that would both result in viable animals and permit time to express the transgene prior to syncytium formation.

For salt feeding assays, age- and sex-matched siblings were transferred into vials containing 2% NaCl food made with Nutri-Fly MF® food base (Genesee Scientific) or control food (*15*). Flies were monitored for survival each day for 10 days.

Tissue Preparation

For fixed imaging, tissues were dissected in PBS and immediately fixed in 3.7% formaldehyde + 0.3% Triton-X for 15 minutes. Immunostaining was performed in 0.3% Triton-X with 1% normal goat serum (*14*). The following antibodies were used: Rabbit anti-GFP (Thermo-Fisher, Waltham MA, A11122, 1:1000), Rat anti-HA (Sigma, 3F10, 1:100), Rabbit anti-Inx3 (generous gift from Reinhard Bauer, 1:75, (*27*)), 488, 568, 633 secondary antibodies (Life Technologies, Alexa Fluor ®, 1:2000). Tissue was stained with DAPI at 5µg/ml and mounted in VECTASHIELD Mounting Media on slides.

Microscopy

Light Microscopy

For fixed imaging, images were obtained on either a Leica SP5 inverted confocal with a 40X/1.25NA oil objective with emission from a 405 nm diode laser, a 488 nm argon laser, a 561 nm Diode laser, and a 633 HeNe laser under control of Leica LAS AF 2.6 software, or on an Andor Dragonfly Spinning Disk Confocal plus. Images were taken with two different cameras, iXon Life 888 1024 x 1024 EMCCD (pixel size 13um) and the Andor Zyla PLUS 4.2 Megapixel sCMOS 2048 x 2048 (pixel size 6.5um) depending on imaging needs. Images were taken on the **40x**/1.25-0.75 oil 11506250: 40X, HCX PL APO, NA: 1.25, Oil, DIC, WD: 0.1mm, coverglass: 0.17mm, Iris diaphragm, Thread type: M25, **63x**/1.20 water 11506279: 63X, HCX PL APO W Corr CS, NA: 1.2, Water, DIC, WD: 0.22mm, Coverglass: 0.14mm-0.18mm, thread type: M25, and **100x**/1.4-0.70 oil 11506210: HCX PL APO, NA: 1.4, Oil, DIC, WD: 0.09mm, Coverglass: 0.17mm, Iris Diaphragm, Thread type: M25. The lasers used were: 405nm diode laser, 488nm argon laser, 561nm diode laser, and HeNe 633nm laser.

For live imaging, hindguts were dissected and cultured based on previous protocols (*14*). Live imaging of cell fusion was performed on a spinning disc confocal (Yokogawa CSU10 scanhead) on an Olympus IX-70 inverted microscope using a 40x/1.3 NA UPlanFl N Oil objective, a 488 nm

and 568 nm Kr-Ar laser lines for excitation and an Andor Ixon3 897 512 EMCCD camera. The system was controlled by MetaMorph 7.7.

Photo-activation was carried out using Leica SP5 and SP8 microscopes and the FRAP Wizard embedded in the Leica AS-F program. An initial z-stack of the tissue was acquired both before and after activation to examine the full extent of PA-GFP movement in three dimensions. PA-GFP was activated by either point activation or region of interest activation with the 405nm laser set to between 5-20%, depending on the microscope and sample of interest. For each imaging session, test activations on nearby tissues were performed prior to quantified experiments to ensure that only single cells were being activated. After activation, the wizard software was used to acquire time lapses of 15s-2min of a single activation plane in order to capture protein movement. Extremely low 488nm and 405nm laser power was used in acquisition of the time lapse images of GFP and Hoechst respectively. Low level 405nm scanning did not significantly activate PA-GFP, and control experiments were performed without the use of 405nm time lapses and showed the same protein movement results (data not shown).

Transmission Electron Microscopy

Hindguts were dissected into PBS and fixed in a solution of 2.5% glutaraldehyde in 0.1% cacodylate buffer, pH 7.2. Post-fix specimens were stained with 1% osmium tetroxide in 0.1M cacodylate buffer, dehydrated, soaked in a 1:1 propylene oxide:Epon 812 resin, and then embedded in molds with fresh Epon 812 resin at 65C overnight. The blocks were cut into semi-thin (0.5µm) sections using Leica Reichert Ultracuts and the sections were stained with 1% methylene blue. After inspection, ultra-thin sections (65nm -75nm) were cut using Leica EM CU7 and contrast stained with 2% uranyl acetate, 3.5% lead citrate solution. Ultrathin sections were visualized on a JEM-1400 transmission electron microscope (JEOL) using an ORIUS (1000) CCD 35mm port camera.

Image Analysis

All image analysis was performed using ImageJ and FIJI (*28, 29*).

Cytoplasm sharing calculation

Cytoplasmic sharing was quantified by manually tracing the total papillar area by morphology and the area marked by mKO2 signal in one z-slice of the papillar face of each animal. The area marked by mKO2 was summed and divided by the sum of the total papillar area to yield the papillar fraction marked by mKO2 which indicates the degree of cytoplasmic sharing within each animal. Papillae without mKO2 signal were excluded from the area measurements.

Line profiles

For line profile data collection, fixed and mounted hindguts were imaged on a Zeiss Apotome on the 40Xoil objective. Once moved into ImageJ, the images were rotated with no interpolation so that the central canal was perpendicular to the bottom of the image. From the midline of the central canal, a straight line (width of 300) was drawn out to one edge of the papillae. One papilla was measured per animal. Papillae were measured at the widest width. Next, the Analyze > Plot Profile data was collected from this representative 300 width line and moved into Excel. In Excel, the data was first was normalized to the maximum length of the papillae and the maximum GFP intensity per animal. Each data point is a % of the total length of the papillae and a % of the maximum GFP intensity. Next, the X values were rounded to its nearest 1% value. Next, all the Y-values were averaged per X value bins (average % GFP intensity per rounded % distance value). % GFP intensity values were plotted from 1-100% total distance of papilla.

Genotype and experiment-specific method notes

Some additional methodological details, including animal genotype, applied to only a specific figure panel. Please see **Table S5** for this information.

Table S1. Cytoplasm sharing primary candidate screen gene results.

Gene category	Gene	Annotation symbol	Gene ID	Sharing disrupted?
Autophagy	*Atg1*	CG10967	FBgn0260945	No
Autophagy	*Atg7*	CG5489	FBgn0034366	No
Autophagy	*Atg8a*	CG32672	FBgn0052672	No
Cell cycle / Chromosomes	*blue*	NA	FBgn0283709	No
Cell cycle / Chromosomes	*CapD2*	CG1911	FBgn0039680	No
Cell cycle / Chromosomes	*Cdc2*	CG5363	FBgn0004106	**Yes**
Cell cycle / Chromosomes	*Clamp*	CG1832	FBgn0032979	No
Cell cycle / Chromosomes	*endos*	CG6513	FBgn0061515	No
Cell cycle / Chromosomes	*fzr*	CG3000	FBgn0262699	**Yes**
Cell cycle / Chromosomes	*Mi-2*	CG8103	FBgn0262519	No
Cell cycle / Chromosomes	*Rbp9*	CG3151	FBgn0010263	No
Cell cycle / Chromosomes	*SA-2*	CG13916	FBgn0043865	No
Cell signaling	*Chico*	CG5686	FBgn0024248	No
Cell signaling	*Egfr*	CG10079	FBgn0003731	**Yes**
Cell signaling	*grk*	CG17610	FBgn0001137	No
Cell signaling	*N*	CG3936	FBgn0004647	No
Cell signaling	*Ptp61F*	CG9181	FBgn0267487	No
Cell signaling	*rho*	CG1004	FBgn0004635	**Yes**
Cell signaling	*ru*	CG1214	FBgn0003295	No
Cell signaling	*spi*	CG10334	FBgn0005672	No
Cell signaling	*stet*	CG33166	FBgn0020248	No
Cell signaling	*wts*	CG12072	FBgn0011739	No
Cell signaling	*βggt-II*	CG18627	FBgn0028970	No
Cytoskeleton	*ALiX*	CG12876	FBgn0086346	No
Cytoskeleton	*Cdc42*	CG12530	FBgn0010341	No
Cytoskeleton	*DCTN1-p150*	CG9206	FBgn0001108	No
Cytoskeleton	*pav*	CG1258	FBgn0011692	No
Cytoskeleton	*wash*	CG13176	FBgn0033692	No
Hindgut-enriched	*dac*	CG4952	FBgn0005677	No
Hindgut-enriched	*Dr*	CG1897	FBgn0000492	No
Hindgut-enriched	*nrv3*	CG8663	FBgn0032946	No
Membrane component	*Flo1*	CG8200	FBgn0024754	No
Membrane component	*Flo2*	CG32593	FBgn0264078	No
Membrane component	*Iris*	CG4715	FBgn0031305	No
Myoblast fusion	*Arf51F*	CG8156	FBgn0013750	No
Myoblast fusion	*Arp2*	CG9901	FBgn0011742	No
Myoblast fusion	*Arp3*	CG7558	FBgn0262716	No
Myoblast fusion	*Ced-12*	CG5336	FBgn0032409	No

Myoblast fusion	*dock*	CG3727	FBgn0010583	No
Myoblast fusion	*hbs*	CG7449	FBgn0029082	No
Myoblast fusion	*Hem*	CG5837	FBgn0011771	No
Myoblast fusion	*mbc*	CG10379	FBgn0015513	No
Myoblast fusion	*Rac1*	CG2248	FBgn0010333	No
Myoblast fusion	*Rho1*	CG8416	FBgn0014020	No
Myoblast fusion	*rols*	CG32096	FBgn0041096	No
Myoblast fusion	*rst*	CG4125	FBgn0003285	No
Myoblast fusion	*SCAR*	CG4636	FBgn0041781	No
Myoblast fusion	*siz*	CG32434	FBgn0026179	No
Myoblast fusion	*WASp*	CG1520	FBgn0024273	No
Polarity	*Abi*	CG9749	FBgn0020510	No
Polarity	*CadN*	CG7100	FBgn0015609	No
Polarity	*cindr*	CG31012	FBgn0027598	No
Polarity	*cno*	CG42312	FBgn0259212	No
Polarity	*Gli*	CG3903	FBgn0001987	No
Polarity	*l(2)gl*	CG2671	FBgn0002121	No
Polarity	*Nrg*	CG1634	FBgn0264975	No
Polarity	*sdt*	CG32717	FBgn0261873	No
Polarity	*shg*	CG3722	FBgn0003391	No
Vesicle trafficking	*Atl*	CG6668	FBgn0039213	No
Vesicle trafficking	*Bet1*	CG14084	FBgn0260857	No
Vesicle trafficking	*Chmp1*	CG4108	FBgn0036805	No
Vesicle trafficking	*CHMP2B*	CG4618	FBgn0035589	No
Vesicle trafficking	*dnd*	CG6560	FBgn0038916	No
Vesicle trafficking	*Exo84*	CG6095	FBgn0266668	**Yes**
Vesicle trafficking	*lerp*	CG31072	FBgn0051072	No
Vesicle trafficking	*Rab11*	CG5771	FBgn0015790	**Yes**
Vesicle trafficking	*Rab23*	CG2108	FBgn0037364	No
Vesicle trafficking	*Rab4*	CG4921	FBgn0016701	No
Vesicle trafficking	*Rab7*	CG5915	FBgn0015795	No
Vesicle trafficking	*Rab8*	CG8287	FBgn0262518	No
Vesicle trafficking	*RabX4*	CG31118	FBgn0051118	No
Vesicle trafficking	*Vha16-1*	CG3161	FBgn0262736	**Yes**
Vesicle trafficking	*Vha55*	CG17369	FBgn0005671	No
Vesicle trafficking	*VhaAC39-1*	CG2934	FBgn0285910	No
Vesicle trafficking	*VhaAC39-2*	CG4624	FBgn0039058	No
Vesicle trafficking	*Vps2*	CG14542	FBgn0039402	**Yes**
Vesicle trafficking	*Vps33b*	CG5127	FBgn0039335	No
Total screen results				
Sharing disrupted	8			
No sharing phenotype	69			
Total	77			

Screen results by category				
Polarity	9			
Vesicle trafficking	19			
Myoblast fusion	15			
Cell cycle / Chromosomes	9			
Cell signaling	11			
Autophagy	3			
Cytoskeleton	5			
Hindgut-enriched	3			
Membrane component	3			
Total	77			

Table S2. Membrane trafficking primary and secondary candidate screen gene results.

Gene category	Gene subcategory	Gene	Annotation symbol	Gene ID	Sharing disrupted?	Screen
Membrane trafficking	ER	*Atl*	CG6668	FBgn0039213	No	Primary
Membrane trafficking	ESCRT	*Chmp1*	CG4108	FBgn0036805	No	Primary
Membrane trafficking	ESCRT	*CHMP2B*	CG4618	FBgn0035589	No	Primary
Membrane trafficking	ESCRT	*Isn*	CG6637	FBgn0260940	No	Secondary
Membrane trafficking	ESCRT	*Vps2*	CG14542	FBgn0039402	**Yes**	Primary
Membrane trafficking	ESCRT	*Vps4*	CG6842	FBgn0283469	No	Secondary
Membrane trafficking	Exocyst	*Exo70*	CG7127	FBgn0266667	No	Secondary
Membrane trafficking	Exocyst	*Exo84*	CG6095	FBgn0266668	**Yes**	Primary
Membrane trafficking	Exocyst	*Sec10*	CG6159	FBgn0266673	**Yes**	Secondary
Membrane trafficking	Exocyst	*Sec15*	CG7034	FBgn0266674	**Yes**	Secondary
Membrane trafficking	Exocyst	*Sec5*	CG8843	FBgn0266670	**Yes**	Secondary
Membrane trafficking	Exocyst	*Sec6*	CG5341	FBgn0266671	**Yes**	Secondary
Membrane trafficking	Exocyst	*Sec8*	CG2095	FBgn0266672	**Yes**	Secondary
Membrane trafficking	Lysosome	*lerp*	CG31072	FBgn0051072	No	Primary
Membrane trafficking	Rab-associated	*CG41099*	CG41099	FBgn0039955	No	Secondary
Membrane trafficking	Rab-associated	*mtm*	CG9115	FBgn0025742	No	Secondary
Membrane trafficking	Rab-associated	*nuf*	CG33991	FBgn0013718	No	Secondary
Membrane trafficking	Rab-associated	*Rala*	CG2849	FBgn0015286	No	Secondary
Membrane trafficking	Rab-associated	*Rep*	CG8432	FBgn0026378	No	Secondary
Membrane trafficking	Rab-associated	*Rip11*	CG6606	FBgn0027335	No	Secondary
Membrane trafficking	Vacuolar H+ ATPase	*Vha16-1*	CG3161	FBgn0262736	**Yes**	Primary
Membrane trafficking	Vacuolar H+ ATPase	*Vha16-2*	CG32089	FBgn0028668	No	Secondary
Membrane trafficking	Vacuolar H+ ATPase	*Vha16-3*	CG32090	FBgn0028667	No	Secondary
Membrane trafficking	Vacuolar H+ ATPase	*Vha16-5*	CG6737	FBgn0032294	**Yes**	Secondary
Membrane trafficking	Vacuolar H+ ATPase	*Vha55*	CG17369	FBgn0005671	No	Primary
Membrane trafficking	Vacuolar H+ ATPase	*VhaAC39-1*	CG2934	FBgn0285910	No	Primary
Membrane trafficking	Vacuolar H+ ATPase	*VhaAC39-2*	CG4624	FBgn0039058	No	Primary
Membrane trafficking	Vacuolar H+ ATPase	*VhaPPA1-1*	CG7007	FBgn0028662	**Yes**	Secondary
Membrane trafficking	Vacuolar H+ ATPase	*VhaPPA1-2*	CG7026	FBgn0262514	**Yes**	Secondary
Membrane trafficking	Vesicle trafficking	*Bet1*	CG14084	FBgn0260857	No	Primary
Membrane trafficking	Vesicle trafficking	*Chc*	CG9012	FBgn0000319	No	Secondary

Membrane trafficking	Vesicle trafficking	*dnd*	CG6560	FBgn0038916	No	Primary
Membrane trafficking	Vesicle trafficking	*shi*	CG18102	FBgn0003392	**Yes**	Secondary
Membrane trafficking	Vesicle trafficking	*Vps29*	CG4764	FBgn0031310	No	Secondary
Membrane trafficking	Vesicle trafficking	*Vps33b*	CG5127	FBgn0039335	No	Primary
Membrane trafficking	Vesicle trafficking	*Vps35*	CG5625	FBgn0034708	No	Secondary
Total screen results						
Sharing disrupted	12					
No sharing phenotype	24					
Total	36					
Screen results by category	**Total**	**Hits**				
ER	1	0				
ESCRT	5	1				
Exocyst	7	6				
Lysosome	1	0				
Rab-associated	6	0				
Vacuolar H+ ATPase	9	4				
Vesicle trafficking	7	1				
Total	36					

Table S3. Primary and secondary candidate screen stock numbers used and results.

Gene	Annotation symbol	Gene ID	Mutant or UAS transgene	Stock Center	Stock Number	Chr	Sharing disrupted?	Notes
Abi	CG9749	FBgn0020510	RNAi	BDSC	51455	2	No	
ALiX	CG12876	FBgn0086346	RNAi	BDSC	33417	3	No	
ALiX	CG12876	FBgn0086346	RNAi	BDSC	50904	2	No	
Arf51F	CG8156	FBgn0013750	RNAi	BDSC	51417	3	No	
Arf51F	CG8156	FBgn0013750	Mutant	BDSC	17076	2	No	
Arf51F	CG8156	FBgn0013750	RNAi	BDSC	27261	3	No	
Arp2	CG9901	FBgn0011742	RNAi	BDSC	27705	3	No	
Arp3	CG7558	FBgn0262716	RNAi	BDSC	32921	3	No	
Atg1	CG10967	FBgn0260945	RNAi	BDSC	44034	2	No	
Atg1	CG10967	FBgn0260945	RNAi	BDSC	26731	3	No	
Atg7	CG5489	FBgn0034366	RNAi	BDSC	34369	3	No	
Atg7	CG5489	FBgn0034366	RNAi	BDSC	27707	3	No	
Atg8a	CG32672	FBgn0052672	RNAi	BDSC	28989	3	No	
Atg8a	CG32672	FBgn0052672	RNAi	BDSC	58309	2	No	
Atg8a	CG32672	FBgn0052672	RNAi	BDSC	34340	3	No	
Atl	CG6668	FBgn0039213	RNAi	BDSC	36736	2	No	
Bet1	CG14084	FBgn0260857	RNAi	BDSC	41927	2	No	
blue	NA	FBgn0283709	RNAi	BDSC	44094	3	No	
blue	NA	FBgn0283709	RNAi	BDSC	41637	2	No	
CadN	CG7100	FBgn0015609	RNAi	BDSC	27503	3	No	
CadN	CG7100	FBgn0015609	RNAi	BDSC	41982	3	No	
CapD2	CG1911	FBgn0039680	Mutant	BDSC	59393	3	No	
Cdc2	CG5363	FBgn0004106	RNAi	VDRC	41838	3	**Yes**	
Cdc2	CG5363	FBgn0004106	RNAi	BDSC	NA	3	No	
Cdc42	CG12530	FBgn0010341	RNAi	BDSC	42861	2	No	
Cdc42	CG12530	FBgn0010341	DN	BDSC	6288	2	No	
Ced-12	CG5336	FBgn0032409	RNAi	BDSC	28556	3	No	
Ced-12	CG5336	FBgn0032409	RNAi	BDSC	58153	2	No	
Chc	CG9012	FBgn0000319	DN	BDSC	26821	2	No	
Chc	CG9012	FBgn0000319	RNAi	BDSC	27350	3	No	
Chc	CG9012	FBgn0000319	RNAi	BDSC	34742	3	No	
Chico	CG5686	FBgn0024248	RNAi	BDSC	36788	2	No	
Chmp1	CG4108	FBgn0036805	RNAi	BDSC	33928	3	No	
CHMP2B	CG4618	FBgn0035589	RNAi	BDSC	28531	3	No	
CHMP2B	CG4618	FBgn0035589	RNAi	BDSC	38375	2	No	
cindr	CG31012	FBgn0027598	RNAi	BDSC	35670	3	No	

cindr	CG31012	FBgn0027598	RNAi	BDSC	38976	2	No	
Clamp	CG1832	FBgn0032979	RNAi	BDSC	27080	3	No	
cno	CG42312	FBgn0259212	RNAi	BDSC	33367	3	No	
cno	CG42312	FBgn0259212	RNAi	BDSC	38194	2	No	
dac	CG4952	FBgn0005677	RNAi	BDSC	26758	3	No	
dac	CG4952	FBgn0005677	RNAi	BDSC	35022	3	No	
DCTN1-p150	CG9206	FBgn0001108	DN	BDSC	51645	2	No	
dnd	CG6560	FBgn0038916	RNAi	BDSC	27488	3	No	
dnd	CG6560	FBgn0038916	RNAi	BDSC	34383	3	No	
dock	CG3727	FBgn0010583	RNAi	BDSC	27728	3	No	
dock	CG3727	FBgn0010583	RNAi	BDSC	43176	3	No	
dock	CG3727	FBgn0010583	Mutant	BDSC	11385	2	No	
Dr	CG1897	FBgn0000492	RNAi	BDSC	26224	3	No	
Dr	CG1897	FBgn0000492	RNAi	BDSC	42891	2	No	
Egfr	CG10079	FBgn0003731	DN	BDSC	5364	2	**Yes**	
Egfr	CG10079	FBgn0003731	RNAi	VDRC	43267	3	**Yes**	
endos	CG6513	FBgn0061515	RNAi	BDSC	53250	3	No	
endos	CG6513	FBgn0061515	RNAi	BDSC	65996	3	No	
Exo70	CG7127	FBgn0266667	RNAi	BDSC	28041	3	No	
Exo70	CG7127	FBgn0266667	RNAi	BDSC	55234	3	No	
Exo84	CG6095	FBgn0266668	RNAi	BDSC	28712	3	**Yes**	
Flo1	CG8200	FBgn0024754	RNAi	BDSC	36700	3	No	
Flo1	CG8200	FBgn0024754	RNAi	BDSC	36649	2	No	
Flo2	CG32593	FBgn0264078	RNAi	BDSC	55212	3	No	
Flo2	CG32593	FBgn0264078	RNAi	BDSC	40833	2	No	
fzr	CG3000	FBgn0262699	RNAi	VDRC	25550	2	**Yes**	
Gli	CG3903	FBgn0001987	RNAi	BDSC	31869	3	No	
Gli	CG3903	FBgn0001987	RNAi	BDSC	58115	2	No	
grk	CG17610	FBgn0001137	RNAi	BDSC	38913	3	No	
hbs	CG7449	FBgn0029082	RNAi	BDSC	57003	2	No	
Hem	CG5837	FBgn0011771	Mutant	BDSC	8752	3	No	
Hem	CG5837	FBgn0011771	Mutant	BDSC	8753	3	No	
Hem	CG5837	FBgn0011771	RNAi	BDSC	29406	3	No	
Hem	CG5837	FBgn0011771	RNAi	BDSC	41688	3	No	
Hsc70Cb	CG6603	FBgn0026418	RNAi	BDSC	33742	3	No	
Hsc70Cb	CG6603	FBgn0026418	DN	BDSC	56497	2	No	
Iris	CG4715	FBgn0031305	RNAi	BDSC	50587	2	No	
Iris	CG4715	FBgn0031305	RNAi	BDSC	63582	2	No	
l(2)gl	CG2671	FBgn0002121	RNAi	BDSC	31517	3	No	
lerp	CG31072	FBgn0051072	RNAi	BDSC	57436	2	No	
lilli	CG8817	FBgn0041111	RNAi	BDSC	26314	3	No	
lilli	CG8817	FBgn0041111	RNAi	BDSC	34592	3	No	
mbc	CG10379	FBgn0015513	RNAi	BDSC	32355	3	No	

mbc	CG10379	FBgn0015513	RNAi	BDSC	33722	3	No	
Mi-2	CG8103	FBgn0262519	RNAi	BDSC	16876	3	No	
mtm	CG9115	FBgn0025742	RNAi	BDSC	38339	3	No	
N	CG3936	FBgn0004647	DN	Rebay Lab	NA	2	No	
N	CG3936	FBgn0004647	RNAi	Sara Bray	NA	1	No	
Nrg	CG1634	FBgn0264975	RNAi	BDSC	28724	3	No	
Nrg	CG1634	FBgn0264975	RNAi	BDSC	38215	2	No	
Nrg	CG1634	FBgn0264975	RNAi	BDSC	37496	2	No	
nrv3	CG8663	FBgn0032946	RNAi	BDSC	29431	3	No	
nrv3	CG8663	FBgn0032946	RNAi	BDSC	50725	3	No	
nuf	CG33991	FBgn0013718	RNAi	BDSC	31493	3	No	
pav	CG1258	FBgn0011692	RNAi	BDSC	35649	3	No	
pav	CG1258	FBgn0011692	RNAi	BDSC	43963	2	No	
Ptp61F	CG9181	FBgn0267487	RNAi	BDSC	32426	3	No	
Ptp61F	CG9181	FBgn0267487	RNAi	BDSC	56036	2	No	
Rab1	CG3320	FBgn0285937	CA	BDSC	9758	3	No	
Rab1	CG3320	FBgn0285937	DN	BDSC	9757	3	**Yes**	Requires 60H12-Gal4
Rab1	CG3320	FBgn0285937	RNAi	BDSC	27299	3	**Yes**	
Rab1	CG3320	FBgn0285937	RNAi	BDSC	34670	3	No	
Rab2	CG3269	FBgn0014009	CA	BDSC	9761	2	No	
Rab2	CG3269	FBgn0014009	DN	BDSC	9759	2	No	
Rab3	CG7576	FBgn0005586	CA	BDSC	9764	3	No	
Rab3	CG7576	FBgn0005586	DN	BDSC	9766	2	No	
Rab4	CG4921	FBgn0016701	CA	BDSC	9770	3	No	
Rab4	CG4921	FBgn0016701	DN	BDSC	9768	2	No	
Rab4	CG4921	FBgn0016701	DN	BDSC	9769	3	No	
Rab5	CG3664	FBgn0014010	CA	BDSC	9773	3	**Yes**	
Rab5	CG3664	FBgn0014010	DN	BDSC	42704	3	**Yes**	Requires 60H12-Gal4
Rab5	CG3664	FBgn0014010	RNAi	BDSC	67877	2	**Yes**	
Rab5	CG3664	FBgn0014010	RNAi	BDSC	30518	3	**Yes**	
Rab5	CG3664	FBgn0014010	RNAi	BDSC	51847	2	No	
Rab6	CG6601	FBgn0015797	CA	BDSC	9776	3	No	
Rab6	CG6601	FBgn0015797	DN	BDSC	23250	3	No	
Rab7	CG5915	FBgn0015795	CA	BDSC	9779	3	No	
Rab7	CG5915	FBgn0015795	DN	BDSC	9778	3	No	
Rab7	CG5915	FBgn0015795	DN	BDSC	9778	3	No	
Rab8	CG8287	FBgn0262518	DN	BDSC	9780	3	No	
Rab8	CG8287	FBgn0262518	CA	BDSC	9781	2	No	
Rab8	CG8287	FBgn0262518	DN	BDSC	9780	3	No	

Rab9	CG9994	FBgn0032782	CA	BDSC	9785	3	No	
Rab9	CG9994	FBgn0032782	DN	BDSC	23642	3	No	
Rab10	CG17060	FBgn0015789	CA	BDSC	9787	3	No	
Rab10	CG17060	FBgn0015789	DN	BDSC	9786	3	No	
Rab11	CG5771	FBgn0015790	CA	BDSC	9791	3	No	
Rab11	CG5771	FBgn0015790	DN	BDSC	23261	3	**Yes**	
Rab11	CG5771	FBgn0015790	RNAi	BDSC	27730	3	**Yes**	
Rab11	CG5771	FBgn0015790	RNAi	VDRC	108382	2	**Yes**	
Rab11	CG5771	FBgn0015790	RNAi	VDRC	22198	3	**Yes**	
Rab11	CG5771	FBgn0015790	Mutant	BDSC	42708	3	**Yes**	
Rab14	CG4212	FBgn0015791	CA	BDSC	9795	2	No	
Rab14	CG4212	FBgn0015791	DN	BDSC	23264	3	No	
Rab18	CG3129	FBgn0015794	CA	BDSC	9797	3	No	
Rab18	CG3129	FBgn0015794	DN	BDSC	23238	3	No	
Rab19	CG7062	FBgn0015793	CA	BDSC	9800	3	No	
Rab19	CG7062	FBgn0015793	DN	BDSC	9799	3	No	
Rab21	CG17515	FBgn0039966	CA	BDSC	23864	2	No	
Rab21	CG17515	FBgn0039966	DN	BDSC	23240	3	No	
Rab23	CG2108	FBgn0037364	RNAi	BDSC	36091	3	No	
Rab23	CG2108	FBgn0037364	RNAi	BDSC	55352	2	No	
Rab23	CG2108	FBgn0037364	CA	BDSC	9806	3	No	
Rab23	CG2108	FBgn0037364	DN	BDSC	9804	3	No	
Rab26	CG34410	FBgn0086913	CA	BDSC	23243	3	No	
Rab26	CG34410	FBgn0086913	DN	BDSC	9808	3	No	
Rab27	CG14791	FBgn0025382	CA	BDSC	9811	2	No	
Rab27	CG14791	FBgn0025382	DN	BDSC	23267	2	No	
Rab30	CG9100	FBgn0031882	CA	BDSC	9814	2	No	
Rab30	CG9100	FBgn0031882	DN	BDSC	9813	3	No	
Rab32	CG8024	FBgn0002567	CA	BDSC	23280	3	No	
Rab32	CG8024	FBgn0002567	DN	BDSC	23281	2	No	
Rab35	CG9575	FBgn0031090	CA	BDSC	9817	3	No	
Rab35	CG9575	FBgn0031090	DN	BDSC	9820	3	No	
Rab39	CG12156	FBgn0029959	CA	BDSC	9823	3	No	
Rab39	CG12156	FBgn0029959	DN	BDSC	23247	3	No	
Rab40	CG1900	FBgn0030391	CA	BDSC	9827	3	No	
Rab40	CG1900	FBgn0030391	DN	BDSC	9829	2	No	
Rab9D	CG32678	FBgn0067052	CA	BDSC	9835	3	No	
Rab9D	CG32678	FBgn0067052	DN	BDSC	23257	2	No	
Rab9E	CG32673	FBgn0052673	CA	BDSC	9832	2	No	
Rab9E	CG32673	FBgn0052673	DN	BDSC	23255	3	No	
Rab9Fb	CG32670	FBgn0052670	CA	BDSC	9844	3	No	
Rab9Fb	CG32670	FBgn0052670	DN	BDSC	9845	2	No	
RabX1	CG3870	FBgn0015372	CA	BDSC	9839	2	No	
RabX1	CG3870	FBgn0015372	DN	BDSC	23252	3	No	

RabX2	CG2885	FBgn0030200	CA	BDSC	9842	3	No	
RabX2	CG2885	FBgn0030200	DN	BDSC	9843	2	No	
RabX4	CG31118	FBgn0051118	RNAi	BDSC	28704	3	No	
RabX4	CG31118	FBgn0051118	RNAi	BDSC	44070	2	No	
RabX4	CG31118	FBgn0051118	CA	BDSC	23277	2	No	
RabX4	CG31118	FBgn0051118	DN	BDSC	9849	3	No	
RabX5	CG7980	FBgn0035255	CA	BDSC	9852	X	No	
RabX5	CG7980	FBgn0035255	DN	BDSC	9853	2	No	
RabX6	CG12015	FBgn0035155	CA	BDSC	9855	2	No	
RabX6	CG12015	FBgn0035155	DN	BDSC	9856	3	No	
CG41099	CG41099	FBgn0039955	RNAi	BDSC	34883	3	No	
Rac1	CG2248	FBgn0010333	RNAi	BDSC	28985	3	No	
Rac1	CG2248	FBgn0010333	DN	BDSC	6292	3	No	
Rala	CG2849	FBgn0015286	DN	BDSC	32094	2	No	
Rala	CG2849	FBgn0015286	RNAi	BDSC	34375	3	No	
Rbp9	CG3151	FBgn0010263	RNAi	BDSC	42796	3	No	
Rep	CG8432	FBgn0026378	RNAi	BDSC	28047	3	No	
rho	CG1004	FBgn0004635	Mutant	BDSC	1471	3	**Yes**	
rho	CG1004	FBgn0004635	RNAi	BDSC	38920	3	**Yes**	
rho	CG1004	FBgn0004635	RNAi	BDSC	41699	2	**Yes**	
Rho1	CG8416	FBgn0014020	DN	BDSC	7328	3	No	
Rho1	CG8416	FBgn0014020	DN	BDSC	58818	2	No	
Rho1	CG8416	FBgn0014020	RNAi	BDSC	32383	3	No	
Rip11	CG6606	FBgn0027335	RNAi	BDSC	38325	3	No	
rols	CG32096	FBgn0041096	RNAi	BDSC	56986	2	No	
rols	CG32096	FBgn0041096	RNAi	BDSC	58262	2	No	
rst	CG4125	FBgn0003285	RNAi	BDSC	28672	3	No	
ru	CG1214	FBgn0003295	RNAi	BDSC	41593	3	No	
ru	CG1214	FBgn0003295	RNAi	BDSC	58065	2	No	
SA-2	CG13916	FBgn0043865	RNAi	VDRC	108267	2	No	
SCAR	CG4636	FBgn0041781	RNAi	BDSC	31126	3	No	
SCAR	CG4636	FBgn0041781	RNAi	BDSC	51803	2	No	
SCAR	CG4636	FBgn0041781	Mutant	BDSC	8754	2	No	
sdt	CG32717	FBgn0261873	RNAi	BDSC	33909	3	No	
sdt	CG32717	FBgn0261873	RNAi	BDSC	35291	3	No	
Sec10	CG6159	FBgn0266673	RNAi	BDSC	27483	3	**Yes**	
Sec15	CG7034	FBgn0266674	RNAi	BDSC	27499	3	**Yes**	
Sec5	CG8843	FBgn0266670	RNAi	VDRC	28873	3	**Yes**	
Sec5	CG8843	FBgn0266670	RNAi	BDSC	50556	3	No	
Sec6	CG5341	FBgn0266671	RNAi	VDRC	105836	2	**Yes**	
Sec6	CG5341	FBgn0266671	RNAi	BDSC	27314	3	**Yes**	
Sec8	CG2095	FBgn0266672	RNAi	BDSC	57441	2	**Yes**	
shg	CG3722	FBgn0003391	RNAi	BDSC	27689	3	No	

shi	CG18102	FBgn0003392	DN	BDSC	5822	3	**Yes**	Requires 60H12-Gal4
shi	CG18102	FBgn0003392	RNAi	BDSC	28513	3	**Yes**	
shi	CG18102	FBgn0003392	RNAi	BDSC	36921	3	**Yes**	
siz	CG32434	FBgn0026179	RNAi	BDSC	39060	2	No	
spi	CG10334	FBgn0005672	RNAi	BDSC	28387	3	No	
spi	CG10334	FBgn0005672	RNAi	BDSC	34645	3	No	
stet	CG33166	FBgn0020248	RNAi	BDSC	57698	3	No	
Vha16-1	CG3161	FBgn0262736	RNAi	BDSC	40923	2	**Yes**	
Vha16-1	CG3161	FBgn0262736	RNAi	VDRC	104490	2	**Yes**	
Vha16-1	CG3161	FBgn0262736	RNAi	VDRC	49291	2	**Yes**	
Vha16-2	CG32089	FBgn0028668	RNAi	BDSC	65167	2	No	
Vha16-3	CG32090	FBgn0028667	RNAi	BDSC	57474	2	No	
Vha16-5	CG6737	FBgn0032294	RNAi	BDSC	25803	3	**Yes**	
Vha55	CG17369	FBgn0005671	RNAi	BDSC	40884	2	No	
VhaAC39-1	CG2934	FBgn0285910	RNAi	BDSC	35029	3	No	
VhaAC39-2	CG4624	FBgn0039058	Mutant	BDSC	62725	3	No	
VhaAC39-2	CG4624	FBgn0039058	RNAi	VDRC	34303	2	No	
VhaPPA1-1	CG7007	FBgn0028662	RNAi	BDSC	57729	2	**Yes**	
VhaPPA1-2	CG7026	FBgn0262514	RNAi	BDSC	65217	2	**Yes**	
Vps2	CG14542	FBgn0039402	RNAi	VDRC	24869	3	**Yes**	
Vps2	CG14542	FBgn0039402	RNAi	BDSC	38995	2	**Yes**	
lsn	CG6637	FBgn0260940	RNAi	BDSC	38289	2	No	
Vps29	CG4764	FBgn0031310	RNAi	BDSC	53951	2	No	
Vps33b	CG5127	FBgn0039335	RNAi	BDSC	44006	2	No	
Vps35	CG5625	FBgn0034708	RNAi	BDSC	38944	2	No	
Vps4	CG6842	FBgn0283469	RNAi	BDSC	31751	3	No	
wts	CG12072	FBgn0011739	RNAi	BDSC	41899	3	No	
wash	CG13176	FBgn0033692	RNAi	BDSC	62866	2	No	
WASp	CG1520	FBgn0024273	RNAi	BDSC	25955	3	No	
WASp	CG1520	FBgn0024273	RNAi	BDSC	51802	2	No	
βggt-II	CG18627	FBgn0028970	RNAi	BDSC	50516	2	No	
βggt-II	CG18627	FBgn0028970	RNAi	BDSC	34902	3	No	

Table S4. Fly stocks used in addition to the screens.

Stock Name	Stock Number	Origin	References
w^{1118}	3605	BDSC	
tub-Gal4	5138	BDSC	
tub-Gal80^{ts}	NA	NA	
UAS-dBrainbow	34513	BDSC	(*12*)
UAS-dBrainbow	34514	BDSC	(*12*)
Hsp70>cre	851	BDSC	
UAS-fzr RNAi	25550	VDRC	(*14,15*)
UAS-shi RNAi #1	28513	BDSC	
UAS-shi RNAi #2	36921	BDSC	
UAS-Rab5 RNAi #1	30518	BDSC	
UAS-Rab5 RNAi #2	67877	BDSC	
UAS-Rab11 RNAi #1	27730	BDSC	
UAS-Rab11 RNAi #2	22198	VDRC	
UAS-SCAR RNAi #1	36121	BDSC	(*30*)
UAS-SCAR RNAi #2	51803	BDSC	(*31*)
UAS-kirre RNAi	27227	VDRC	(*32*)
UAS-sns RNAi	877	VDRC	(*32*)
UAS-schizo RNAi	36625	VDRC	(*33*)
UAS-sing RNAi	12202	VDRC	(*34*)
UAS-Cdc42^{DN}	6288	BDSC	
UAS-Rac1^{DN}	6292	BDSC	
UAS-Rho1^{DN}	7328	BDSC	
UAS-GFP-NLS	4776	BDSC	
UAS-GFP-Myc-2x-FYVE	42712	BDSC	(*35, 36*)
UAS-YFP-Rab5	9775	BDSC	
60H12-Gal4	39268	BDSC	
UAS-shi^{DN}	5811	BDSC	
NrxIV-GFP	50798	BDSC	
Df(1)BSC867	29990	BDSC	
UAS-ogre RNAi	7136	VDRC	(*37, 38*)
byn-Gal4	-	NA	(*39*)
UAS-PA-GFP	-	Lynn Cooley	(*40*)
UAS-N^{DN}	-	NA	(*41*)
UAS-shi-Venus	-	Stefano De Renzis	(*42*)
UAS-GFP-ogre	-	Andrea Brand	(*38*)

Table S5. Additional Methods.

Panel	Additional Methods
1D-D''	*Hsp70>cre ; UAS-dBrainbow ; byn-Gal4* papillae dissected at 62 (D), 69 (D'), or 80 (D'') hours post-puparium formation (HPPF) at 25C. Hindguts were stained with Rabbit anti-GFP (Thermo-Fisher, A11122, 1:1000), Rat anti-HA (Sigma, 3F10, 1:100), and DAPI at 5µg/ml.
1E	*Hsp70>cre ; UAS-dBrainbow ; byn-Gal4* papillae dissected at various HPPF at 25C. The area labelled by mKO2 was divided by total papillar area.
1F	*Hsp70>cre ; UAS-dBrainbow ; byn-Gal4* papillae live-imaged at 69HPPF at 25C.
1F'	Fluorescence intensity measured in neighboring cells during sharing onset (1F).
1G-H	*byn-Gal4 / UAS-PA-GFP*, live-imaged during adulthood. Single secondary and primary cells were photoactivated and imaged every 3s.
2A	UAS-RNAis and dominant-negative versions of 77 genes representing a wide range of cellular roles were screened (*Hsp70>cre* ; *UAS-dBrainbow* ; *byn-Gal4*) for sharing defects. Animals expressing both *UAS-dBrainbow* and an *UAS*-driven RNAi or mutant gene were raised at 25C and shifted to 29C at L3. If a given RNAi or DN line was lethal when expressed with the *byn-Gal4* driver, a $Gal80^{ts}$ was crossed in and the animals raised at 18C with a shift to 29C at pupation. Given the robustness of cytoplasmic sharing in WT animals, gene knockdowns or mutants with even single cell defects in sharing were considered "hits".
2B	Secondary screen of 36 genes representing various categories of membrane trafficking (*Hsp70>cre* ; *UAS-dBrainbow* ; *byn-Gal4*) for sharing defects. Animals expressing both *UAS-dBrainbow* and an *UAS*-driven RNAi were raised at 25C and shifted to 29C at L3. If a given RNAi line was lethal when expressed with the *byn-Gal4* driver, a $Gal80^{ts}$ was crossed in and the animals raised at 18C with a shift to 29C at pupation. Given the robustness of cytoplasmic sharing in WT animals, gene knockdowns with even single cell defects in sharing were considered "hits".
2C	Secondary screen (*Hsp70>cre* ; *UAS-dBrainbow* ; *byn-Gal4*) of dominant-negative and constitutively-active variants of the *Drosophila* Rab GTPases. $UAS\text{-}Rab11^{DN}$ and $UAS\text{-}Rab14^{DN}$ required a $Gal80^{ts}$ repressor and temperature shifts from 18C to 29C at pupation. $UAS\text{-}Rab1^{DN}$ and $UAS\text{-}Rab5^{DN}$ required papillar-specific expression using an alternative *Gal4* driver (*60H12-Gal4*), $Gal80^{ts}$ repressor, and temperature shifts from 18C to 29C at pupation.
2D	*Hsp70>cre* ; *UAS-dBrainbow* ; *byn-Gal4,* $Gal80^{ts}$ animals dissected pre-sharing (48 HPPF at 29C).
2D'	*Hsp70>cre* ; *UAS-dBrainbow* ; *byn-Gal4,* $Gal80^{ts}$ animals raised at 18C and shifted to 29C at pupation and dissected post-sharing (young adult).
2E	Young adult animals expressing *UAS-shi RNAi #1* in a *Hsp70>cre* ; *UAS-dBrainbow* ; *byn-Gal4,* $Gal80^{ts}$ background. Animals were shifted from 18C to 29C at pupation to maximize RNAi and minimize animal lethality.
2F	Young adult animals expressing *UAS-Rab5 RNAi #1* in a *Hsp70>cre* ; *UAS-dBrainbow* ; *byn-Gal4,* $Gal80^{ts}$ background. Animals were shifted from 18C to 29C at 1-2 days PPF to maximize RNAi and minimize animal lethality.

2G	Young adult animals expressing *UAS-Rab11 RNAi #2* in a *Hsp70>cre* ; *UAS-dBrainbow* ; *byn-Gal4, Gal80^{ts}* background. Animals were shifted from 18C to 29C at 1-2 days PPF to maximize RNAi and minimize animal lethality.
2H	Animals were shifted and dissected as in 2D-G. Additionally, *Hsp70>cre* ; *UAS-dBrainbow* ; *byn-Gal4, Gal80^{ts}* animals expressing *UAS-shi RNAi #2* were raised at 18C and shifted to 29C at pupation, animals expressing *UAS-Rab5 RNAi #2* were raised at 18C and shifted to 29C at L3, and animals expressing *UAS-Rab11 RNAi #1* were raised at 18C and shifted to 29C at 1-2 days PPF.
3A-A'	Pupae expressing the early and late endosome marker *UAS-GFP-myc-2x-FYVE* were dissected pre (A, 48HPPF at 29C) and post (A', 72HPPF at 29C) sharing onset.
3B	Pupae expressing *UAS-GFP-myc-2x-FYVE* in a *UAS-shi RNAi #1* background at a post sharing time point (24HPPF at 18C + 72 hours at 29C).
3C	Aggregated line profiles of *UAS-GFP-myc-2x-FYVE* intensity across papilla.
3D-D'	Pupae expressing *UAS-shi-Venus* were dissected pre (D, 48HPPF at 29C) and post (D', 72HPPF at 29C) sharing onset.
3E	Aggregated line profiles of Shi-Venus intensity from the basal (0% distance) to the apical (100% distance) edges of the papilla. See 3C.
3F-F"	Transmission electron micrographs of the microvillar-like structures of pupal papillae pre (F, 60HPPF at 25C), mid (F', 66HPPF at 25C), and post (F'', 69HPPF at 25C) cytoplasm sharing onset.
3G-G"	Electron micrographs of mitochondria and surrounding membrane material pre (G, 60HPPF at 25C), mid (G', 66HPPF at 25C), and post (G'', 69HPPF at 25C)
3H	Electron micrograph of microvillar-like structures of WT (*w^{1118}*) young adult papillar cells.
3I	Electron micrograph of microvillar-like structures of young adult *byn-Gal4, Gal80^{ts} > UAS-shi RNAi #2* (raised at 18C, shifted at pupation to 29C).
3J	Electron micrograph of microvillar-like structures of young adult *byn-Gal4, Gal80^{ts} > UAS-Rab5 RNAi #1* animals (raised at 18C, shifted at 1-2 days PPF to 29C).
3K	Electron micrograph of mitochondria and surrounding membrane material of WT (*w^{1118}*) young adult papillar cells.
3L	Electron micrograph of mitochondria and surrounding membrane material of young adult *byn-Gal4, Gal80^{ts} > UAS-shi RNAi #2* (raised at 18C, shifted at pupation to 29C).
3M	Electron micrograph of mitochondria and surrounding membrane material of young adult *byn-Gal4, Gal80^{ts} > UAS-Rab5 RNAi #1* animals (raised at 18C, shifted at 1-2 days PPF to 29C).
3N	Electron micrograph of post-sharing WT (TM3 / *UAS-shi RNAi #1*) pupa (24HPPF at 18C, shifted to 29C for 50 hours, then dissected)
3O	Electron micrograph of post-sharing *byn-Gal4, Gal80^{ts} > UAS-shi RNAi #1* pupa (24HPPF at 18C, shifted to 29C for 50 hours, then dissected)
3P	Gap junction length / (gap junction length + septate junction length) measured in WT and *UAS-shi RNAi #1* pupae (see 3N-3O). Each point represents an image of a junction.
4A-A"	Electron micrographs of apical junctions (adherens, septate, and gap) pre (A, 60HPPF at 25C), mid (A', 66HPPF at 25C), and post (A'', 69HPPF at 25C)
4B	Gap junction length / (gap junction length + septate junction length) measured in pupae pre (60HPPF at 25C), mid (66HPPF at 25C), and post (69HPPF at 25C) sharing onset. Each point represents an image of a junction.

4C	Relative innexin transcript abundance (innexin X transcripts / total innexin transcripts) using data from Fly Atlas 2 (*25*) and RNA-seq of adult w^{1118} rectums performed in the Fox Lab.
4D-D'	Pupae with endogenously GFP-tagged NrxIV (*NrxIV-GFP*) dissected pre (D, 48HPPF) and post (D', 72HPPF) sharing onset.
4E-E'	Pupae stained with Inx3 antibody (gift from Reinhard Bauer, rabbit, 1:75) pre (D, 48HPPF) and post (D', 58HPPF, papillae do not stain well at later timepoints) sharing onset.
4F	Young adult animals expressing no transgene (WT), *UAS-ogre*^{DN}, *UAS-ogre RNAi*, or containing a deficiency covering *ogre*, *Inx2*, and *Inx7* in a *Hsp70>cre ; UAS-dBrainbow ; byn-Gal4, Gal80*^{ts} background. Animals were raised at 25C until L3 and then shifted to 29C until dissection at young adulthood.
4G	See 4F.
4H	*60H12-Gal4*, *Gal80*^{ts} driving *UAS-shi*^{DN} and WT siblings were shifted from 18C to 29C at pupation. *byn-Gal4, Gal80*^{ts} driving *UAS-ogre*^{DN} animals and WT siblings were raised at 25C and shifted to 29C at L3. Animals 1-3 days post-eclosion were sorted into sex-matched groups and fed a control diet or a high salt (2% NaCl) diet. Survival was assessed once per day for 10 days.
S1A	*Hsp70>cre ; UAS-dBrainbow ; tubulin-Gal4* animals raised at 29C. Tissues dissected at adulthood.
S1E	*Hsp70>cre* ; UAS-*dBrainbow* ; *byn-Gal4* animals were shifted from 25C to 29C during L3 and dissected at adulthood.
S1F	*Hsp70>cre* ; UAS-*dBrainbow* / *UAS-fzr RNAi* ; *byn-Gal4* animals were shifted from 25C to 29C during L2 to maximize *fzr* knock down during endocycling. Animals were dissected at adulthood.
S1G	*Hsp70>cre ; UAS-dBrainbow ; byn-Gal4 / UAS-N*^{DN} animals were shifted from 25C to 29C during L3 to ensure maximum *UAS-N*^{DN} expression during mitoses. Animals were dissected at adulthood.
S2A	*Hsp70>cre* ; *UAS-dBrainbow* ; *byn-Gal4, Gal80*^{ts} animals expressing various previously published myoblast fusion RNAis raised at 25C and shifted to 29C at L3 and dissected post-sharing (young adult).
S2B	*Hsp70>cre* ; *UAS-dBrainbow* ; *byn-Gal4, Gal80*^{ts} animals expressing various previously published UAS-dominant negative active regulators raised at 18C and shifted to 29C at L3 and dissected post-sharing (young adult).
S2C	Papillar cells were identified using *byn-Gal4, Gal80*^{ts}, driving *UAS-GFP*^{NLS} expression. Cells were counted in one, z-sectioned half of the papillae and multiplied by 2 to give an approximate cell count.
S2D	*Hsp70>cre* ; *UAS-dBrainbow* ; *byn-Gal4, Gal80*^{ts} animals were raised at 18C until 3-4 days PPF and shifted to 29C and dissected at young adulthood.
S2E	*Hsp70>cre* ; *UAS-dBrainbow* ; *byn-Gal4, Gal80*^{ts} animals expressing *UAS-shi RNAi #1* were raised at 18C until 3-4 days PPF and shifted to 29C and dissected at young adulthood.
S3A	See 3A-3C. Basal and apical membrane defined as 10-20% and 90-100% total distance of papillae, respectively.
S3B-B'	*byn-Gal4 > UAS-Rab5-YFP* animals dissected pre (48HPPF, 29C) and post (72HPPF, 29C) sharing onset.
S3C	See S3B-B' and 3C.

S3D-D"	Electron micrographs of apical junctions (adherens, septate, and gap) pre (D, 60HPPF at 25C), mid (D', 66HPPF at 25C), and post (D'', 69HPPF at 25C)
S3E	Electron micrograph of apical junctions (adherens, septate, and gap) of WT (w^{1118}) young adult papillar cells.
S3F	Electron micrograph of apical junctions (adherens, septate, and gap) of young adult *byn-Gal4, Gal80^{ts} > UAS-shi RNAi #2* (raised at 18C, shifted at pupation to 29C).
S3G	Electron micrograph of apical junctions (adherens, septate, and gap) of young adult *byn-Gal4, Gal80^{ts} > UAS-Rab5 RNAi #1* animals (raised at 18C, shifted at 1-2 days PPF to 29C).
S3H	See 3N-O. Junction width was measured throughout and averaged per image. Each point represents one image of a junction.
S3H'	See 3N-O. Junction width was measured throughout and averaged per image. Each point represents one image of a junction.
S3H"	See 3N-O. Raw lengths shown were used to calculate "fraction gap junction" in 3P. Each point represent one image of a junction.
S4A	TEM of young adult (w^{1118}) papilla.
S5A	See 4A-B. Junction width was measured throughout and averaged per image. Each point represents one image of a junction.
S5A'	See 4A-B. Junction width was measured throughout and averaged per image. Each point represents one image of a junction.
S5A"	See 4A-B. Raw lengths shown were used to calculate "fraction gap junction" in 3P. Each point represent one image of a junction.
S5B-B'	Pupae expressing *byn-Gal4, Gal80^{ts} > UAS-ogre^{DN}* (*UAS-GFP-ogre*) dissected pre (B, 48HPPF, 29C) and post (B', 72HPPF, 29C) sharing onset.
S5C	*byn-Gal4 > UAS-GFP^{NLS}* dissected pre (48HPPF, 29C) sharing onset.
S5D	*60H12-Gal4 > UAS-GFP^{NLS}* dissected pre (48HPPF, 29C) sharing onset. The pan-hindgut driver used in previous experiments, *brachyenteron* (*byn*>Gal4), causes animal lethality with *shi*, *Rab5*, and *Rab11* knockdown within a few days. We therefore screened for and identified an alternative, papillae-specific driver (*60H12*>Gal4), derived from regulatory sequences of the hormone receptor gene *Proctolin Receptor. 60H12>shi^{DN}* animals are viable on a control diet allowing us to test papillar function on a high-salt diet.
S5E	*Hsp70>cre ; UAS-dBrainbow ; 60H12-Gal4* animals raised at 18C and shifted to 29C at pupation and dissected as young adults.
S5F	*Hsp70>cre ; UAS-dBrainbow ; 60H12-Gal4 / UAS-shi^{DN}* animals raised at 18C and shifted to 29C at pupation and dissected as young adults.
S5G	See S5E-F.

Table S6. Additional statistics.

Panel	N range	Reps	Statistical test	P-value
1E	9-18	2	Unpaired t-test	66HPPF:74HPPF <0.0001
2H	9-32	2-3	One-way ANOVA with Tukey's multiple comparisons test	ANOVA: <0.0001 Pre:WT <0.0001 WT:*shi #1* <0.0001 WT:*shi #2* <0.0001 WT:*Rab5 #1* <0.0001 WT:*Rab5 #2* <0.0001 WT:*Rab11 #1* <0.0001 WT:*Rab11 #2* <0.0001 *shi #1*:*Rab5 #2* 0.0181 *shi #1*:*Rab11 #2* 0.0428 *shi #2*:*Rab5 #2* 0.0263 *Rab5 #1*:*Rab5 #2* 0.0009 *Rab5 #1*:*Rab11 #2* 0.0020 all others, ns
3C	6-10	2-3	see S3A	see S3A
3E	4-5	3	Unpaired t-test	Apical region: Pre:Post <0.0001
3P	3-4	2	Unpaired t-test	WT:*shi RNAi* <0.0001
4B	3-4	2	Unpaired t-test	Pre:Post <0.0001
4F	13-14	2	One-way ANOVA with Tukey's multiple comparisons test	ANOVA: <0.0001 WT:$ogre^{DN}$ <0.0001 WT:*Df* <0.0001 WT:*ogre RNAi* 0.0007
4H	27-37	3	One-way ANOVA with Tukey's multiple comparisons test (mean death at 10 days in each group)	ANOVA: <0.0001 WTsalt:shi^{DN}reg ns, 0.7173 WTsalt:shi^{DN}salt <0.0001 shi^{DN}salt:shi^{DN}reg <0.0001 ANOVA: <0.0001 WTsalt:$ogre^{DN}$reg <0.0001 WTsalt:$ogre^{DN}$salt <0.0001 $ogre^{DN}$salt:$ogre^{DN}$reg <0.0001
S1H	12-20	2	Unpaired t-test	WT:*fzr RNAi* <0.0001 WT:N^{DN} ns, 0.1786
S2A	8-11	2	One-way ANOVA with Tukey's multiple comparisons test	ANOVA: <0.0001 *Sing RNAi*:all others <0.0001 All others: ns
S2B	2-3	1	One-way ANOVA	ANOVA: ns, 0.5488

S2C	11-23	2	One-way ANOVA with Tukey's multiple comparisons test	ANOVA: 0.0044 *shi RNAi #1*:*Rab11 RNAi #1* 0.0244 *Rab5 RNAi #2*:*Rab11 RNAi #1* 0.0193 All others: ns
S2F	10-11	2	Unpaired t-test	ns, 0.0782
S3A	6-10	2	One-way ANOVA with Tukey's multiple comparisons test	ANOVA: <0.0001 Pre:Post <0.0001 Pre:*shi RNAi* ns, 0.7882 Post:*shi RNAi* <0.0001
S3C	10	2	Unpaired t-test	Apical basal difference (see S3A) Pre:Post 0.0007
S3H	3-4	2	Unpaired t-test	ns, 0.2203
S3H'	3-4	2	Unpaired t-test	ns, 0.4754
S3H''	3-4	2	Multiple unpaired t-tests	Septate: WT:*shi RNAi* ns, 0.1547 Gap: WT:*shi RNAi* <0.0001
S5A	3-4	2	One-way ANOVA	ns, 0.8973
S5A'	3-4	2	One-way ANOVA	ns, 0.3994
S5A''	3-4	2	Multiple unpaired t-tests	Septate: all ns Gap: Pre:Post 0.0004 Gap: all others, ns
S5G	11	2	Unpaired t-test	WT:shi^{DN} <0.0001

SUPPLEMENTAL FIGURE LEGENDS

Figure S1. The hindgut rectal papillae share cytoplasm independent of mitosis.

(**A**) Representative images of dBrainbow expression in the indicated adult tissues. (**B**) Schematic of cytoplasmic sharing quantification. The mKO2-positive papillar area is divided by the total papillar area to give a score of cytoplasmic sharing. Numbers close to 1 indicate near-complete sharing. (**C**) Schematic of principal cells (sharing) and secondary cells (non-sharing) at the papillar base that together form each papilla. (**D**) Approximate timeline of cytoplasm sharing onset (68-74 HPPF) within papillar development (*14*). Cytoplasmic sharing is temporally separate from papillar mitoses. (**E-G**) Representative adults expressing dBrainbow in a (**E**) wild-type (WT), (**F**) *fzr RNAi* ($p<0.0001$), or (**G**) N^{DN} background ($p=0.8786$). (**H**) Quantification of cytoplasmic sharing in adult WT, *fzr RNAi*, and N^{DN}-expressing animals (N=12-20, rep=2).

Figure S2. Membrane trafficking genes expressed during a developmental window regulate cytoplasm sharing.

(**A**) Quantification of cytoplasmic sharing in animals expressing dsRNA for myoblast fusion regulators (N=8-11, rep=2). All knockdown lines are previously published (*30-34*). Only *sing RNAi* significantly differs from WT ($p<0.0001$). (**B**) Quantification of cytoplasmic sharing in animals expressing dsRNA for Rho family GTPases. (**C**) Cell counts in WT and knockdown rectal papillae (N=11-23, rep=2). Only *Rab11 #1 RNAi* had a significantly different cell number than WT ($p=0.0323$). (**D-E**) Representative animals expressing *dBrainbow* in either a WT (**D**) or *shi RNAi* (**E**) genetic background were raised at 18C until 3-4 days PPF and shifted to 29C to induce *shi*

knockdown at a later timepoint than in **Figure 2E, 2H**. (**F**) Sharing quantification in late-induced animals (N=10-11, rep=2).

Figure S3. Changes in endosome polarity and apical junction shape accompany the onset of cytoplasm sharing.

(**A**) Quantification of the average endosome intensity difference between representative basal and apical areas across papillae in **Figure 3A-C** (N=6-10, rep=2). (**B-B'**) Representative localization of Rab5-YFP, green, before sharing onset (**B**) and after sharing onset (**B'**). (**C**) Aggregated line profiles of Rab5-YFP intensity before and after the beginning of sharing (N=10, rep=2). (**D-D''**) Representative TEMs of apical (adherens, septate, and gap) junctions pre (**D**), mid (**D'**), and post (**D''**) sharing onset. (**E-G**) Representative TEMs of apical junctions of post-sharing adult WT (**E**), *shi RNAi* (**F**), and *Rab5 RNAi* (**G**) papillar cells. (**H-H''**) Apical junction electron micrograph measurements of post-sharing WT and *shi RNAi* pupal papillar cells (N=3-4, rep=2). Average gap junction (**H**) and septate junction (**H'**) widths were measured alongside gap and septate junction length. Width measurements were taken along the length of each cell-cell junction and averaged to give one point per cell-cell junction. (**H''**) Raw septate and gap junction lengths (nm) that were used to calculate gap junction ratio in **Figure 3P**.

Figure S4. Extracellular spaces separate nuclei throughout much of the papillar lateral membrane.

(**A**) Representative TEM cross-section of an adult WT papilla.

Figure S5. Gap junction formation coincides with cytoplasm sharing onset.

(**A-A''**) Apical junction TEM measurements of pre, mid, and post-sharing onset pupal papillar cells (N=3-4, rep=2). Average gap junction (**A**) and septate junction (**A'**) widths were measured

alongside gap and septate junction length. (**A''**) Raw septate and gap junction lengths (nm) used to calculate gap junction ratio in **Figure 4B**. (**B-B'**) Gap junction localization visualized by *UAS-GFP-ogre* in pre (**B**) and post (**B'**) sharing onset pupae. (**C**) Representative image of *byn-Gal4* driving GFP^{NLS} expression throughout the pre-sharing hindgut. (**D**) *60H12-Gal4* driving GFP^{NLS} expression in pre-sharing papillae but not in the ileum or pylorus. (**E**) Representative image of *60H12-Gal4* driving dBrainbow in adult papillae. (**F**) Representative image of *60H12-Gal4* driving shi^{DN} expression in a dBrainbow background in adult papillae. (**G**) Quantification of cytoplasm sharing in *60H12-Gal4* and *60H12-Gal4>*shi^{DN} animals (N=11, rep=2). (**H**) Model of membrane and junctional changes requiring membrane trafficking genes that coincide with the onset of cytoplasm sharing.

REFERENCES AND NOTES

27. C. Lehmann *et al.*, Heteromerization of innexin gap junction proteins regulates epithelial tissue organization in Drosophila. *Mol Biol Cell* **17**, 1676-1685 (2006).
28. C. T. Rueden *et al.*, ImageJ2: ImageJ for the next generation of scientific image data. *Bmc Bioinformatics* **18**, (2017).
29. J. Schindelin *et al.*, Fiji: an open-source platform for biological-image analysis. *Nat Methods* **9**, 676-682 (2012).
30. M. Bischoff *et al.*, Cytonemes are required for the establishment of a normal Hedgehog morphogen gradient in Drosophila epithelia. *Nat Cell Biol* **15**, 1269-1281 (2013).
31. G. Xing *et al.*, Neurexin-Neuroligin 1 regulates synaptic morphology and functions via the WAVE regulatory complex in Drosophila neuromuscular junction. *Elife* **7**, (2018).
32. G. A. Linneweber, M. Winking, K. F. Fischbach, The Cell Adhesion Molecules Roughest, Hibris, Kin of Irre and Sticks and Stones Are Required for Long Range Spacing of the Drosophila Wing Disc Sensory Sensilla. *PLoS One* **10**, e0128490 (2015).
33. R. I. Johnson, A. Sedgwick, C. D'Souza-Schorey, R. L. Cagan, Role for a Cindr-Arf6 axis in patterning emerging epithelia. *Mol Biol Cell* **22**, 4513-4526 (2011).
34. T. M. Brunetti, B. J. Fremin, R. M. Cripps, Identification of singles bar as a direct transcriptional target of Drosophila Myocyte enhancer factor-2 and a regulator of adult myoblast fusion. *Developmental Biology* **401**, 299-309 (2015).
35. D. J. Gillooly *et al.*, Localization of phosphatidylinositol 3-phosphate in yeast and mammalian cells. *Embo J* **19**, 4577-4588 (2000).
36. T. Wucherpfennig, M. Wilsch-Brauninger, M. Gonzalez-Gaitan, Role of Drosophila Rab5 during endosomal trafficking at the synapse and evoked neurotransmitter release. *J Cell Biol* **161**, 609-624 (2003).
37. C. E. Holcroft *et al.*, Innexins Ogre and Inx2 are required in glial cells for normal postembryonic development of the Drosophila central nervous system. *J Cell Sci* **126**, 3823-3834 (2013).
38. P. Speder, A. H. Brand, Gap junction proteins in the blood-brain barrier control nutrient-dependent reactivation of Drosophila neural stem cells. *Dev Cell* **30**, 309-321 (2014).
39. J. B. Singer, R. Harbecke, T. Kusch, R. Reuter, J. A. Lengyel, Drosophila brachyenteron regulates gene activity and morphogenesis in the gut. *Development* **122**, 3707-3718 (1996).
40. S. R. Datta *et al.*, The Drosophila pheromone cVA activates a sexually dimorphic neural circuit. *Nature* **452**, 473-477 (2008).
41. I. Rebay, R. G. Fehon, S. Artavanistsakonas, Specific Truncations of Drosophila Notch Define Dominant Activated and Dominant-Negative Forms of the Receptor. *Cell* **74**, 319-329 (1993).
42. P. Fabrowski *et al.*, Tubular endocytosis drives remodelling of the apical surface during epithelial morphogenesis in Drosophila. *Nat Commun* **4**, 2244 (2013).

Figure S1

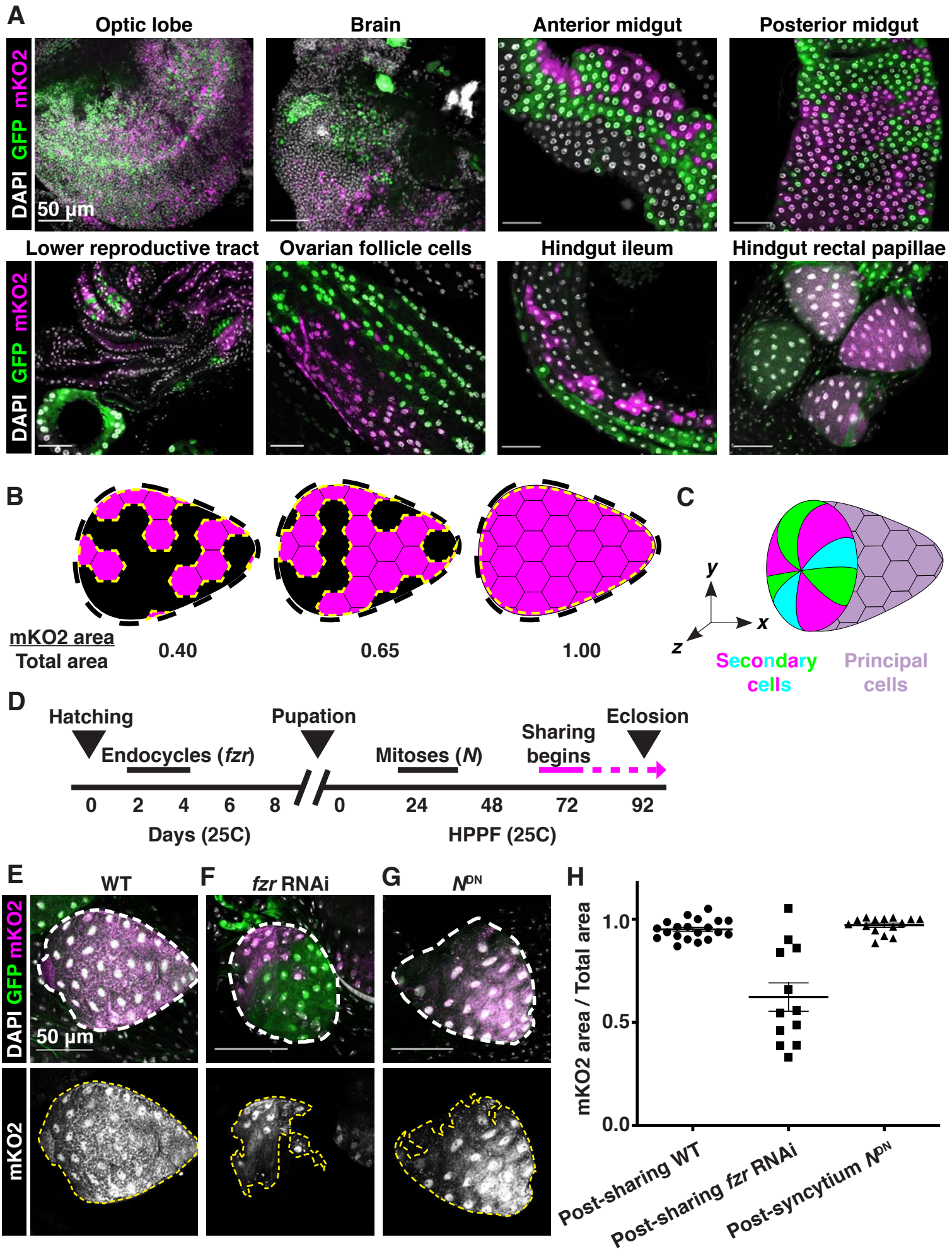

Figure S2

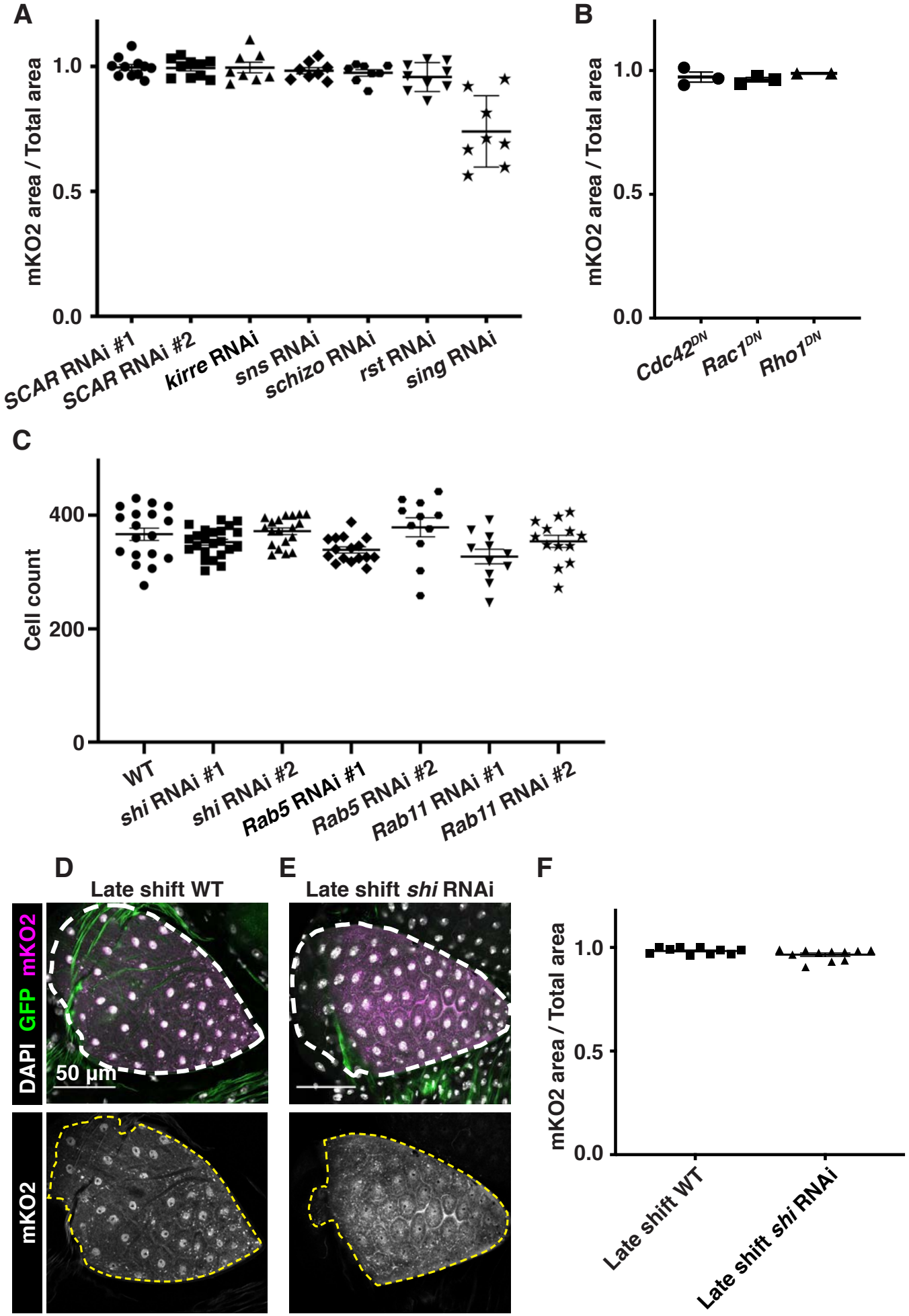

Figure S3

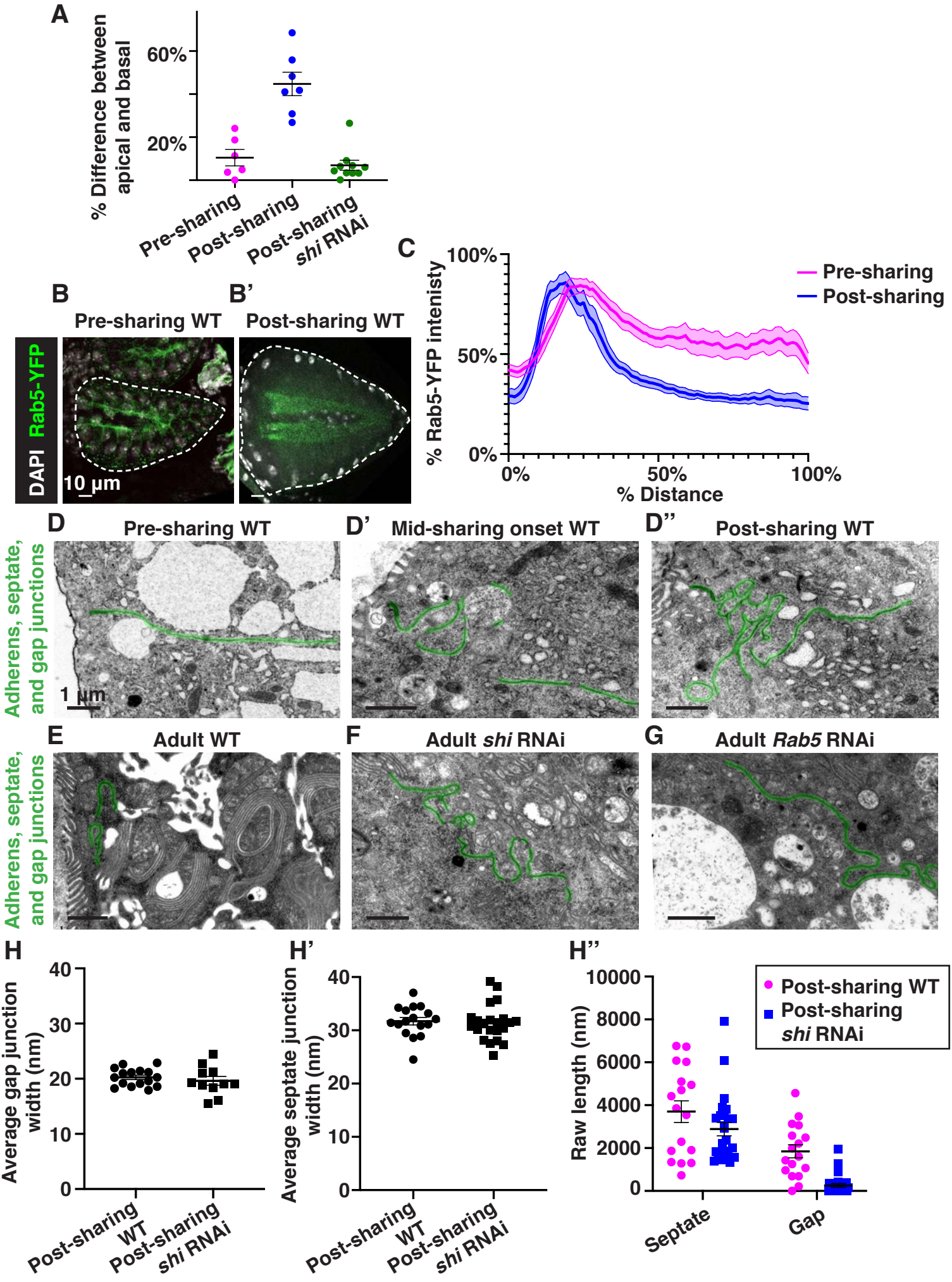

Figure S4

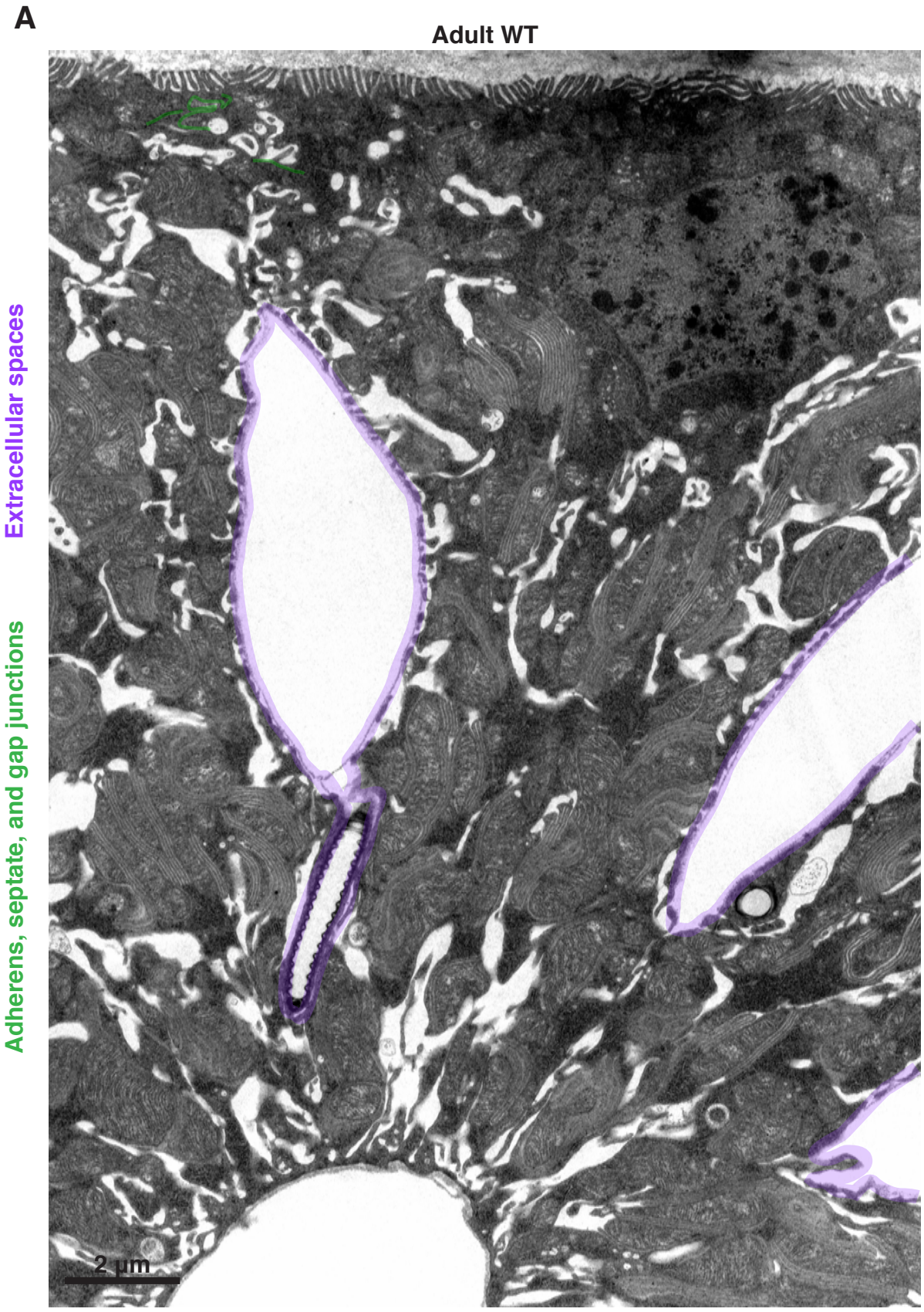

Figure S5